Lecture notes on superconducting quantum circuits

Juan José García-Ripoll (*)
Borja Peropadre

(*) jj.garcia.ripoll@csic.es

October 1, 2014

Preface

What you have in your hands is some version of a set of lecture notes in the theory of superconducting circuits and its applications to Quantum Optics, Quantum Information and Quantum Simulation. The notes have been started in September the 1st, 2014, with the excuse of a Quantum Optics school that will take place in Benasque, in October 2014. This means that some of you will read a partially finished version of the notes, and some of you will read a more elaborate set of notes, hopefully with less typos and notational inconsistencies.

If you are reading one of the earliest versions, I beg your forgiveness, for the lack of time is forcing me to write these notes in a rather conversational manner, as the topics spun out of my head, and trying to be consistent among sections, but without much time to revisit the material once written. In this case, or even in the case in which get to a more elaborate version, I welcome your feedback on the structure, content and presentation of the different topics.

The content of the notes is quite diverse and it is selected with a strongly biased view of the field and focusing on the personal interests of the author, some of which are already spelled above. The emphasis is not so much on the topics of Quantum Computation, algoritmia and similar ideas, which are beautifully spelled somewhere else, but on the tools that one has needed to enter and enjoy the blooming field of superconductor quantum optics.

Juan José García-Ripoll
September 5, 2014
Madrid, Spain

Contents

Notation

C	Capacitance
E_J	Josephson energy
L	Inductance
$\mathcal{L}$	Lagrangian or Lindblad operator
$\Phi_0 = \frac{h}{2e}$	Magnetic flux quantum
$\varphi_0 = \frac{\Phi}{2\pi} = \frac{\hbar}{2e}$	Flux to phase conversion
ϕ	Flux on a node of a circuit §2.1
$\delta\phi$	Flux on a branch of a circuit §2.1
	Linear capacitor
	Linear inductor
	Nonlinear inductance associated to a Josephson junction
	Josephson junction: nonlinear inductor and capacitor in parallel
	Constant voltage source.

Chapter 1

Introduction

Chapter 2

Quantum circuit theory

2.1 Quantization procedure

The quantization of a superconducting circuit is obtained through the following set of rules, that start with the classical circuit theory, expressed in terms of flux variables, constructs an effective Lagrangian, derives a Hamiltonian and quantizes it using canonically conjugate variables. The procedure is reminiscent of the canonical quantization of moving particles within a non-relativistic setup, but involves some additional considerations that merge-in ideas from circuit theory and the Kirchhoff laws. Our quantization procedure is essentially the one found in the lecture notes by M. Devoret in [Dev95], though we will apply it to a larger family of examples and discuss certain subtleties that lay outside the actual rules.

1. **Labelling:** Identify all distinct nodes in the circuit, which are those intersections where different circuital elements connect. All points in the same line of a circuit are considered to be equivalent and thus a line without circuital elements (capacitors, inductors, etc) cannot have more than one node.

2. **Build the tree:** We will select a starting node, which will typically be a ground plane, and build an open and directed tree that runs through all nodes in the circuit, without creating loops.

3. **Branch fluxes on the tree:** To each circuital element in the

previous tree will associate a flux, $\delta\phi_{ij} = \phi_j - \phi_i$, the difference between the end (j) and initial points (i) of the branch, taking into consideration the orientation that we chose for the branch.

4. **Flux quantization:** The remaining circuital elements will be the ones that close different superconducting loops. The flux on those branches will satisfy a quantization equation

$$\sum_{b\in\text{loop}} \delta\phi_b + \Phi_{loop} = n\Phi_0, \tag{2.1}$$

where Φ_{loop} is the magnetic flux that runs through the loop, $\Phi_0 = h/2e$ is the flux quantum and n is any integer number that represents the trapped quanta of vorticity (typically zero if the system was properly annealed).

5. **Branch currents:** Once we have the branch fluxes identified, we can establish the currents that go through the branches using the appropriate relations shown below:

$$\begin{aligned} &\text{Capacitor} && I = C\dot{V} = C\delta\ddot{\phi} \\ &\text{Inductor} && \dot{I} = V/L \Rightarrow I = \delta\phi/L \\ &\text{Junction} && I = -L_J\varphi_0 \sin(\delta\phi/\varphi_0) \end{aligned}$$

Here L_J is the junction inductance to first order and $E_J = L_J\varphi_0^2$ is the Josephson energy.

6. **Current conservation:** For each node, there will be an equation denoting the fact that the sum of all currents converging to that node is zero:

$$I_C + I_L + I_J = 0, \tag{2.2}$$

where I_C, I_L, and I_J are the currents associated to the inductive, capacitive and Josephson junction elements. In practice this will be a set of differential equations that can be written in the form

$$\sum_{ij\in\text{capacitor}} C_{ij}\delta\ddot{\phi}_{ij} + \sum_{ij\in\text{inductor}} \frac{\delta\phi_{ij}}{L_{ij}} + \sum_{ij\in\text{junction}} \frac{E_J}{\varphi_0}\sin(\delta\phi_{ij}/\varphi_0) = 0. \tag{2.3}$$

In this equation we have a capacitance and inductance matrices, C and $(1/L)$, as well as nonlinear elements representing the Josephson junctions.

7. **Lagrangian:** The differential equations associated to (2.2) can be derived from an effective Lagrangian $\mathcal{L}$ via the variational equations
$$\frac{d}{dt}\frac{\partial \mathcal{L}}{\partial \dot{\phi}_i} = \frac{\partial \mathcal{L}}{\partial \phi_i} \tag{2.4}$$
This Lagrangian has to be reversed engineered from the differential equations in terms of the flux variables.

8. **Canonical variables:** From the Lagrangian we btain the charge variables as the canonically conjugate momenta to the respective fluxes
$$q_i = \frac{\partial \mathcal{L}}{\partial \dot{\phi}_i} \tag{2.5}$$
We will impose that each pair of flux-charge variables satisfy the canonical commutation relations
$$[\phi_i, q_j] = i\hbar\delta_{ij}, \tag{2.6}$$
and evolve according to the Hamiltonian
$$H = \sum_i q_i \dot{\phi}_i - \mathcal{L}, \tag{2.7}$$
expressed solely in terms of these $\{q_i, \phi_i\}$ variables (i.e. replacing $\dot{phi}_i$ with its expressions in terms of charges).

2.2 Practical examples

The following subsections list a number of circuits that are either needed for the understanding of microwave photons and superconducting qubits, or which are complicated enough that they represent **useful exercises** in the application of the superconducting circuit quantization theory. Except for a few paradigmatic circuits, such as the DC-SQUID, we do not discuss anything but the design of the equivalent circuit, the finding of the appropriate variables and the resulting Lagrangian and Hamiltonian. In this sense, this section represents a more up-to-date complement to the excellent notes by M. Devoret [Dev95]. Finally, the interested reader is advised to read this section by looking first at the introductory paragraph and circuits, and **try to derive the resulting equations** herself, thereby correcting the lack of solved problems in these notes.

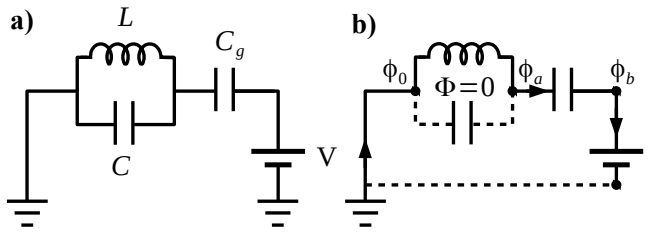

Figure 2.1: (a) Equivalent circuit for an LC resonator consisting on an inductor in parallel with a capacitor, subject to an external potential $V(t)$. (b) Nodes and fluxes for the circuit description and quantization. Note that the value of the flux ϕ_b is imposed by the external potential $\dot{\phi}_b = V(t)$.

2.2.1 LC resonator

In figure 2.1 we show the equivalent circuit for a superconducting resonator that is externally driven by a voltage source. The elements in the circuit are: (i) the capacitor C and (ii) the inductor L which are in parallel; (iii) the external voltage source and (iv) the capacitor that couples it to the resonator, C_g.

In figure 2.1b we have selected the set of nodes, starting with the ground plane and running to the right until the voltage source is reached. Note how this creates a directed and open tree, with only two distinct node variables, ϕ_a and ϕ_b, as the ground plane flux ϕ_0 can be set to zero without loss of generality. Note also that we are going to assume that there is no flux trapped in the resonator, though this does not significantly alter the resulting equations. As a consequence, the flux on the upper branch is equal to the lower branch. Finally, the presence of the voltage source imposes a constraint on the flux $\frac{d}{dt}\phi_b = V$.

We now write down an equation that balances the incoming intensities from the branches to the left and to the right of the a-node:

$$C_J\ddot{\phi}_a + \frac{1}{L}\phi_a = C_g(\dot{V} - \ddot{\phi}_a), \tag{2.8}$$

where $C_\Sigma = C_J + C_g$ is the total capacitance. We can regroup terms

$$C_\Sigma \left(\dot{\phi}_a - \frac{C_g}{C_\Sigma} \dot{V} \right) = \frac{1}{L} \phi_a \tag{2.9}$$

This equation is conservative and derived from an effective Lagrangian via (2.4). The Lagrangian is found to be, up to irrelevant constants,

$$L = \frac{1}{2} C_\Sigma (\dot{\phi}_a - V)^2 + \frac{1}{2L} \phi_a^2. \tag{2.10}$$

The charge operator is obtained from the capacitive terms

$$q_a = C_\Sigma (\phi_a - V) \tag{2.11}$$

and the Hamiltonian is obtained using the Legendre transform

$$H = q_a \dot{\phi}_a - \mathcal{L} = \frac{1}{2C_\Sigma} q^2 + \frac{C_g}{C_\Sigma^2} qV + \frac{1}{2L} \phi_a^2 \tag{2.12}$$

Note that the previous Hamiltonian may be written, up to a c-number

$$H = \frac{1}{2C_\Sigma} \left(q_a - q_g \right)^2 + \frac{1}{2L} \phi_a^2 \tag{2.13}$$

with the externally induced charge $q_g = C_g V / C_\Sigma$.

2.2.2 Transmission line

The next most important circuit that we need to analyze is a superconducting cable that is capable of transporting microwave energy. There are many circuits that can do that, from coaxial cables that are similar to the ones transporting our TV signal, to simple superconducting lines imprinted on a chip, in top of a ground plane. The uses and designs of these lines will be discussed later in §3.3.

In this section we are only concerned with the equivalent circuit describing those microwave guides, which is an array of coupled LC-resonators, similar to the one in figure 2.2. In this circuit, the capacitors represent the electric energy that is stored between the cable and the ground plane that surrounds it (a metallic network in the case of a coaxial cable or a superconducting ground plane in other cases), while the inductors represent the natural impedance of the cable towards changes

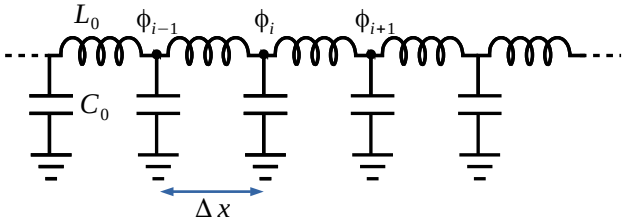

Figure 2.2: Equivalent circuit for a transmission line or a coplanar waveguide. The line is discretized as a set of coupled resonators, each of size Δx and with capacitances and inductances $C_0 = \Delta x \times c_0$, $L_0 = \Delta x \times l_0$. The tree starts in the ground plane and spans, as a star, to all nodes by the vertical capacitors. Because there are no actual loops, there are also no "trapped" fluxes.

in the current. Note that the equivalent circuit is a discretized version of the line, where the resonators have a size Δx that is much smaller than both the wavelength and the actual length of the conductor. For consistency, the capacitance and inductance per resonator are defined in terms of some capacitance and inductance densities, c_0 and l_0, as in

$$C_0 = c_0 \Delta x, \; L_0 = l_0 \Delta x. \tag{2.14}$$

The quantization procedure for this circuit is rather simple. We start by identifying all connections to ground with the same node, $\phi_0 = 0$, and build the tree as a star that spans without loops to all nodes in the line, labeled $\{\phi_1, \phi_2 \dots \phi_N\}$. Current conservation on the nodes leads to the equations[1]

$$\frac{1}{L_0}(\phi_i - \phi_{i-1}) + \frac{1}{L_0}(\phi_{i+1} - \phi_i) + C_0 \ddot{\phi}_i = 0. \tag{2.15}$$

This equation can be derived from a simple Lagrangian

$$\mathcal{L} = \sum_{i=1}^{N} \frac{1}{2} C \dot{\phi}_i^2 - \sum_{i=1}^{N-1} \frac{1}{2L} (\phi_{i+1} - \phi_i)^2. \tag{2.16}$$

[1]Note that while each two consecutive nodes with a ground plane form a "loop" in our model, in the physical implementation there are no such loops and thus we need not consider trapped fluxes.

Because of our choice of tree, the capacitive terms are local and the charges are simply defined as the charge difference between a given point in the line and the corresponding one on the ground plane

$$q_i = \frac{\partial \mathcal{L}}{\partial \dot{\phi}_i} = C\dot{\phi}_i. \tag{2.17}$$

The Hamiltonian consequently is a simple sum of capactive and inductive energies

$$H = \sum_{i=1}^{N} q_i \dot{\phi}_i - \mathcal{L} = \sum_{i=1}^{N} \frac{1}{2C_0} q_i^2 + \sum_{i=1}^{N-1} \frac{1}{2L_0}(\phi_{i+1} - \phi_i)^2. \tag{2.18}$$

The continuum limit of this theory is obtained by inserting the actual size of the discretization

$$H = \sum_{i=1}^{N} \frac{\Delta x}{2c_0} \left(\frac{q_i}{\Delta x}\right)^2 + \sum_{i=1}^{N-1} \frac{\Delta x}{2l_0} \left(\frac{\phi_{i+1} - \phi_i}{\Delta x}\right)^2. \tag{2.19}$$

Using the charge density, $\rho(x_i) = q_i/\Delta x$, and replacing sums with integrals we obtain the usual quadratic field theory

$$H = \int \mathrm{d}x \left\{ \frac{1}{2c}\rho(x)^2 + \frac{1}{2l}[\partial_x \phi(x)]^2 \right\}, \tag{2.20}$$

where now the commutation relation is $[\phi(x), \rho(y)] = i\hbar\delta(x - y)$.

2.2.3 Charge qubit

In figure 2.3 we show the equivalent circuit for a superconducting island that is coupled to a ground plane via a Josephson junction. The elements in the circuit are: (i) the capacitor describing the interaction between the island and the plane, (ii) the capacitor C_g describing the interaction with an electrode that applies a voltage V onto the island, (iii) the Josephson junction E_J allowing pairs to hop in and out of the island. In this figure we appreciate the similarities with the LC resonator, the only significant difference being the nonlinear inductance associated to the Josephson junction.

The quantization procedure for the charge qubit is equivalent to the one we followed for the LC resonator in §2.2.1. The choice of

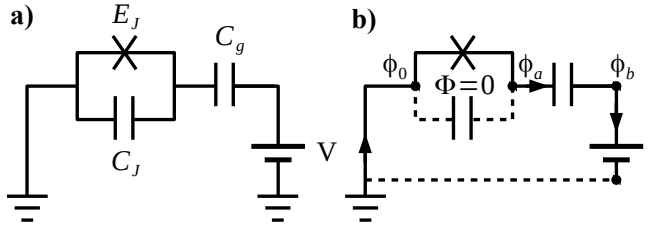

Figure 2.3: Equivalent circuit for the charge qubit, with the actual network on the right. The superconducting island is the region contained between the two capacitors, C_J and C_g. The nonlinear element E_J represents the channel by which pairs can tunnel into the ground plane.

nodes and fluxes is identical, and the only difference is in the current-voltage relation of the Josephson junction, which leads to the following nonlinear differential equation:

$$C_J\ddot{\phi}_a + (E_J/\varphi_0)\sin(\phi_a/\varphi_0) = C_g(\dot{V} - \ddot{\phi}_a), \tag{2.21}$$

The associated Lagrangian is modified accordingly to include the nonlinear inductive energy of the junction

$$L = \frac{1}{2}C_\Sigma(\dot{\phi}_a - V)^2 + E_J\cos(\phi_a/\varphi_0). \tag{2.22}$$

The charge operator is the same as before and the Hamiltonian looks identical except for the change in the inductance

$$H = \frac{1}{2C_\Sigma}q^2 + \frac{C_g}{C_\Sigma^2}qV - E_J\cos(\phi_a/\varphi_0), \tag{2.23}$$

Note that once more the previous Hamiltonian may be written, up to a c-number

$$H = \frac{1}{2C_\Sigma}\left(q - q_g\right)^2 - E_J\cos(\phi_a/\varphi_0), \tag{2.24}$$

with the externally induced charge $q_g = C_gV/C_\Sigma$ shifting the equilibrium state of the qubit.

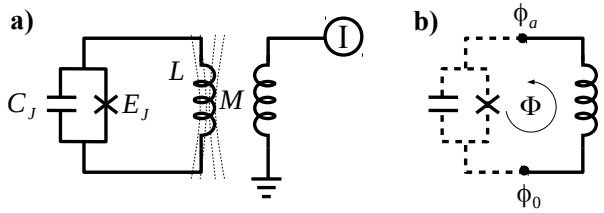

Figure 2.4: Equivalent circuit for the RF-squid qubit in full version (a) or restricted to the SQUID (b). A Josephson junction (C_J, E_J) is shorted by a large inductor L which may couple to an external magnetic field generated by a current source. The mutual inductance M is introduced in the text.

2.2.4 RF-SQUID

A Josephson junction may not only be associated to a capacitor, but also to an inductor. The circuit that results from short-circuiting a junction with a large inductor (a longer "cable") is shown in figure 2.4. The resulting device is called an RF-SQUID, where SQUID stands for Superconducting Quantum Interference Device, and it is one of the earliest designs for qubits. We are interested on this design mainly because it introduces two new ingredients for the first time:

1. the possibility of coupling different superconductors through a magnetic interaction, hereby denoted as M or mutual inductance, and

2. the possibility of threading an external flux inside the superconducting, having $\Phi \neq 0$ for the first time.

Based on the first point, the current conservation on the upper node is written in terms of the branch flux on the inductor, $\phi_L = \phi_a - \phi_0$ and the flux on the junction, ϕ_J

$$C_J \ddot{\phi_J} + \frac{E_J}{\varphi_0} \sin(\phi_J/\varphi_0) = L\phi_L + MI. \tag{2.25}$$

This equation takes into account the mutual inductance between both circuits, with the external current source modifying the current on the large loop.

The greatest complication arises now, because the second point above forces us to distinguish between ϕ_J and ϕ_L, relating them only through the quantization relation

$$\phi_L + \phi_J + \Phi = n\Phi_0. \tag{2.26}$$

The important question is: what value of Φ do we have to introduce in this equation in order to clear ϕ_J? The answer is that Φ, the magnetic flux, arises as a sum of external contributions induced by devices such as the external inductor in figure 2.4, and therefore proportional to the mutual inductance, $\propto MI$, plus the magnetic field generated from the supercurrents in the circuit itself, which we typically neglect in the small circuits we deal with. We will therefore write, assuming no trapped fluxes,

$$\phi_J = -\phi_L - \Phi. \tag{2.27}$$

The dynamical equation of the circuit is therefore

$$-C_J\ddot{\phi_L} - \frac{E_J}{\varphi_0}\sin\left[\frac{1}{\varphi_0}(\phi_L + \Phi)\right] = L\phi_L - MI \tag{2.28}$$

This equation can be reordered to adopt the form 2.4 with a Lagrangian

$$\mathcal{L} = \frac{1}{2}C_J\dot{\phi}^2 - \frac{1}{2L}\phi^2 + M\phi I + E_J\cos\left[\frac{1}{\varphi_0}(\phi + \Phi)\right], \tag{2.29}$$

and its associated Hamiltonian (up to c-numbers)

$$H \simeq \frac{1}{2C_J}q^2 + \frac{1}{2L}(\phi - MLI)^2 + E_J\cos\left[\frac{1}{\varphi_0}(\phi + \Phi)\right]. \tag{2.30}$$

As we will argue below, not all terms have to be considered in practice: ML can be very small when compared with the effective displacement in Φ induced by the external current I.

2.2.5 DC-SQUID

The word SQUID means Superconducting QUantum Interference Device. This denomination is most evident in a design with multiple Josephson junctions, such as the DC-SQUID shown in figure 2.5a, where two junctions are connected in parallel. As in the case of the

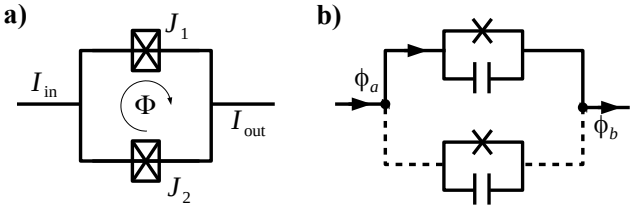

Figure 2.5: (a) A DC-SQUID is a device consisting on two junctions in parallel, threaded by some magnetic flux. (b) A more detailed version of the circuit must take into account the capacitive and inductive energy of the junctions if the pair is unbalanced.

RF-SQUID, we have to consider the flux quantization and the flux induced by external fields or by the supercurrent in the ring itself.

The quantization of the loop proceeds as before, but we are going to consider the possibility of having currents injected in and out of the squid. Current conservation on both nodes imposes $I_{out} = I_{in} = I$ so that we only have to worry about one equation. Moreover, flux quantisation imposes a difference between the fluxes above, $\delta\phi_u = \delta\phi_b - \delta\phi_a$, and below, $\delta\phi_d$,

$$\delta\phi_u + \delta\phi_d + \Phi_{ext} = 0. \tag{2.31}$$

As said above, we only need one differential equation that summarizes the total intensity across the SQUID

$$C_{J1}\delta\ddot{\phi}_u - \frac{E_{J1}}{\varphi_0}\sin(\delta\phi_u/\varphi_0) = C_{J1}\delta\ddot{\phi}_d - \frac{E_{J1}}{\varphi_0}\sin(\delta\phi_d/\varphi_0) + I$$

We assume that the junctions are all identical to simplify the calculation

$$C(\delta\ddot{\phi}_u - \delta\ddot{\phi}_d) = -\frac{E_J}{\varphi_0}2\sin\left(\frac{\delta\phi_d - \delta\phi_u}{2\varphi_0}\right)\sin\left(\frac{\delta\phi_d + \delta\phi_u}{2\varphi_0}\right) + I \tag{2.32}$$

We can define two effective fluxes, $\phi_\pm = \frac{1}{2}(\delta\phi_d \pm \delta\phi_u)$. The first flux, $\phi_+ = -\Phi_{ext}/2$, is related to the circulating flux in the SQUID, while the flux difference ϕ_- is related to the current that passes through the

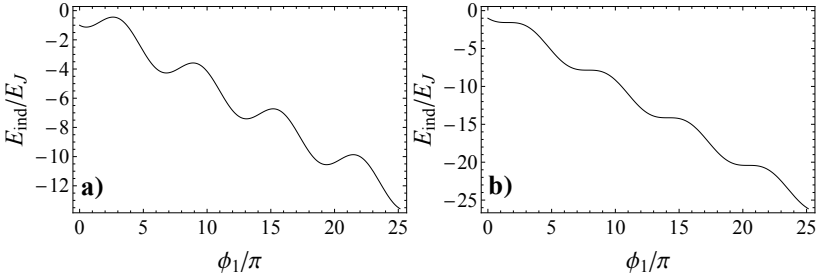

Figure 2.6: Washboard potential of the DC-SQUID (2.35) (a) below and (b) on the verge of switching to a voltage state.

device. The effective Lagrangian in this case is

$$\mathcal{L} = \frac{1}{2} 2C\dot{\phi}_-^2 + 4E_J \cos\left(\frac{\phi_-}{\varphi_0}\right) \cos\left(\frac{\Phi}{2\varphi_0}\right) + I\phi_- \tag{2.33}$$

DC-SQUID as a tunable junction

The effective Lagrangian of the DC-SQUID from equation 2.33 is very similar to that of a single Josephson junction. The main differences are (i) the total capacitance is the sum of the capacitances of both junctions and (ii) the effective Josephson energy is modulated by the external flux

$$E_J(\Phi) = E_J(0) 2 \sin(\Phi/\varphi_0). \tag{2.34}$$

This idea is indeed used pervasively in the circuit-QED community, from the design of charge qubits (§4.2) or transmon (§4.4), to the design of microwave resonators, where the SQUID acts as a tunable inductance that can be used to dynamically change the resonator frequency.

DC-SQUID as a magnetometer

One of the main applications of the DC-SQUID is to do extremely magnetic field measurements. The basic idea stems from the inductive potential associated to the SQUID (2.35)

$$E_{ind} = -4E_J \cos\left(\frac{\phi_-}{\varphi_0}\right) \cos\left(\frac{\Phi}{2\varphi_0}\right) - I\phi_- \tag{2.35}$$

This curve forms a washboard potential such as the one plotted in figure 2.6a. In this stage, contemplating the SQUID as a classical object, there are infinitely many equivalent metastable configurations in the minima of the potential. All these minima represent situations of constant flux, $\phi_- \sim 0$, and therefore no potential, $V \propto \dot{\phi}_- = 0$.

However, if the externally induced bias intensity I reaches the critical value $I_c = 4E_J \cos(\Phi/2\varphi_0)/\varphi_0$, all minima disappear (cf. figure 2.6a) and the state of the SQUID becomes deconfined, the flux growing quadratically in time and giving rise to a potential difference that also grows between nodes a and b in figure 2.5b.

Note that the quantum prediction in the unstable case $I > I_c$ is unphysical and also undesirable. In practice, for the purposes of magnetometry, the DC-SQUID is designed so that both junctions have a similar resistance. This has the effect of stabilizing the washboard potential, driving the voltage states to the minima and preventing tunneling to the continuum, while in the unstable case it restricts the maximum potential that can be reached. Under these conditions, the potential difference assimilates to a sinusoidal function of the externally applied flux, $V_{ab} \propto \cos(\Phi)$, varying at a scale, the flux quantum Φ_0, that implies an extremely good sensitivity.

2.2.6 Three-junction flux qubit

The next level of complexity in the circuit design arises when we consider not two, but three Josephson junctions [cf. Figure 2.7a. As in the case of the RF-squid and DC-squid, the flux quantisation plays an important role, as does the choice of normal modes or collective variables to describe the loop.

Instead of following all the quantisation rules, since we are already familiar with the protocol, we may write down the equations for the branch fluxes shown in figure 2.7b. Flux quantisation allows us to eliminate one branch variable

$$\delta\phi_1 + \delta\phi_2 + \delta\phi_3 + \Phi = 0, \tag{2.36}$$

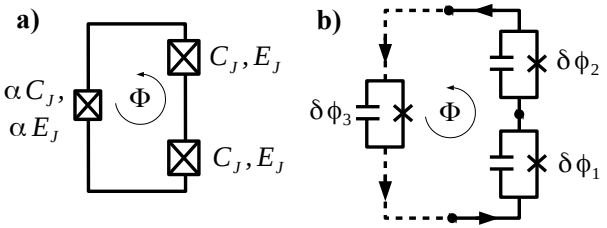

Figure 2.7: (a) The qubit is a loop with three Josephson junctions, two identical $(1, 2)$ and a smaller one (3). (b) The equivalent circuit where we focus only on the branch fluxes.

so that the equations become

$$\begin{aligned} I_{loop} &= -\frac{E_{J3}}{\varphi_0}\sin(\Phi - \delta\phi_1 - \delta\phi_2) - C_{J3}(\delta\ddot{\phi}_1 + \delta\ddot{\phi}_2) \quad (2.37) \\ &= -\frac{E_{J1}}{\varphi_0}\sin(\delta\phi_1) + C_{J1}\delta\ddot{\phi}_1 \\ &= -\frac{E_{J2}}{\varphi_0}\sin(\delta\phi_2) + C_{J2}\delta\ddot{\phi}_2. \end{aligned}$$

Assuming that two of the junctions are balanced, $C_{J1} = C_{J2} = C_J$ and $E_{J1} = E_{J2} = E_J$, and the third one is smaller, $E_{J3} = \alpha E_J, C_{J3} = \alpha C_J$. We can thereafter introduce flux "center of mass" and difference,

$$\phi_\pm = \delta\phi_1 \pm \delta\phi_2, \quad (2.38)$$

and add and subtract equations, to arrive at

$$\begin{aligned} \frac{1}{2}(1+2\alpha)C_J\ddot{\phi}_+ &= \frac{\alpha E_J}{\varphi_0}\sin(\Phi - \phi_+) - \frac{E_J}{\varphi_0}\sin\left(\frac{\phi_+}{2\varphi_0}\right)\cos\left(\frac{\phi_-}{2\varphi_0}\right) \\ C_J\ddot{\phi}_- &= -\frac{E_J}{\varphi_0}\cos\left(\frac{\phi_+}{2\varphi_0}\right)\sin\left(\frac{\phi_-}{2\varphi_0}\right) \end{aligned}$$

Integrating these equations, we obtain the Lagrangian

$$\begin{aligned} \mathcal{L} &= \frac{1}{2}(1/2+\alpha)C_J\dot{\phi}_+^2 + \frac{1}{2}C_J\dot{\phi}_-^2 \quad (2.39) \\ &+ \alpha E_J\cos\left(\frac{\Phi - \phi_+}{\varphi_0}\right) + 2E_J\cos\left(\frac{\phi_+}{2\varphi_0}\right)\cos\left(\frac{\phi_-}{2\varphi_0}\right), \end{aligned}$$

with the associated Hamiltonian

$$\begin{aligned} H &= \frac{1}{2(1/2+\alpha)C_J}q_+^2 + \frac{1}{2C_J}q_-^2 \\ &- \alpha E_J \cos\left(\frac{\Phi-\phi_+}{\varphi_0}\right) - 2E_J \cos\left(\frac{\phi_+}{2\varphi_0}\right)\cos\left(\frac{\phi_-}{2\varphi_0}\right), \end{aligned} \tag{2.40}$$

Chapter 3

Microwave photons

3.1 Energy quantization and photons

The LC-resonator is the simplest nontrivial superconducting circuit that one may build with non-dissipative elements. Classically the resonator acts as a harmonic oscillator, with energy

$$E = \frac{1}{2C}q^2 + \frac{1}{2L}\phi^2 \tag{3.1}$$

and with the flux and charge variables, or voltage and intensity, oscillating at the frequency

$$\omega_{LC} = \frac{1}{\sqrt{LC}}. \tag{3.2}$$

Quantum mechanically we expect this resonator to be quantized. In other words, the system will exhibit a discrete but infinite set of stationary states with energy

$$E_n = \hbar\omega\left(n + \frac{1}{2}\right), \quad n \in \{0, 1, 2\ldots\} \tag{3.3}$$

and the exchange of energy with the environment and other circuits will only be done in quanta of $\hbar\omega$.

The quantisation of energy in the LC resonator extends also to all other linear circuits, such as cables or waveguides. In all these cases, there exist bosonic excitations that we will call *microwave photons*,

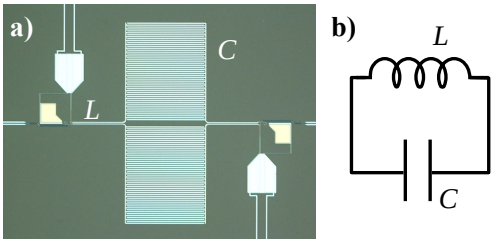

Figure 3.1: (a) A resonator formed by an interdigitated fingers capacitor and a short line that acts as an inductor. Courtesy of Pol Forn-Díaz, IQC, Canada. (b) Equivalent circuit.

which can be emitted to the environment (radiated) or exchanged with the substrate, impurities or other circuits. While conducted through the superconductor, or in between superconducting planes, these photons are combined excitations of the electromagnetic field and the surface currents on the superconductor that move with them. That's fine: it only affects the speed of such excitations, which move slightly slower than in true vacuum, but still follow similar wave equations and exhibit similar dispersion relations.

These and other ideas are the topic of this chapter, where we start with the LC-resonator, introducing the tools to diagonalize and find the quantisation of its energy levels. We then move on to transmission lines or waveguides through which photons move freely and demand a quantum field theory to be described. Of course, the quantisation of the electromagnetic field demands other tools, such as measurement apparatus that can either detect photons or track their fluctuations, which will be the topic of later chapters.

3.2 LC resonator

Figure 3.1a shows an example of an LC-resonator as one would have it in mind: a large, very well identified capacitor with many finger providing room to store charge, connected in parallel with some superconducting loop providing additional inductance. In figure 3.1b we provide a simplified version of the equivalent circuit that was already obtained in 2.2.1 and which we will now quantize.

In order to study the simplified resonator without external voltage sources, we take $C_g = 0$ in the models from §2.2.1, obtaining the Hamiltonian from equation 3.1. The quantization of the flux and charge variables (2.6) establishes an analogy between charge-flux and momentum-position that allows us to diagonalize the Hamiltonian using Fock creation and anihilation operators, a and $a^\dagger$,

$$H = \hbar\omega(a^\dagger a + \tfrac{1}{2}), \tag{3.4}$$

$$\phi_a = \sqrt{\frac{\hbar Z}{2}}(a + a^\dagger), \tag{3.5}$$

$$q_a = \sqrt{\frac{\hbar}{2Z}}i(a^\dagger - a), \tag{3.6}$$

with the oscillator frequency from (3.2), and an oscillator wavepacket length $a_0 = \sqrt{\hbar Z}$ that is proportional to the impedance $Z = \sqrt{L/C}$.

Note how the capacitance C plays the role of the mass in the oscilator, while the inductance L plays the role of the inverse trapping strength of a harmonic potential (i. e. the smaller the inductance, the larger the inductive energy, the tighter the potential). Both combined give rise to the quantisation of the oscilator energy in units of the frequency $\omega = (LC)^{-1/2}$, meaning that the electric energy that is confined in the resonator and which typically belongs to the microwave regime (MHz-GHz), can only be extracted or inserted in units or "photons" with energy $\hbar\omega$. The commutation relations of the Fock operators a and $a^\dagger$ that anihilate and create these quasiparticles can be derived from those of ϕ and q,

$$[a, a^\dagger] = 1 \tag{3.7}$$

and manifest the excitations of the resonator are bosons. Both features, quantization and bosonic statistics, justify the name "photons".

Phase space dynamics

The behavior of the flux and charge variables is completely equivalent to those of the position and momentum operator in the harmonic oscillator. From equation (3.4) we can obtain the evolution equations of the Fock operators in the Heisenberg picture

$$\frac{d}{dt}O = i[H, O], \tag{3.8}$$

which substituting a and $a^\dagger$ for O and using $[a, a^\dagger] = 1$, have as solutions

$$a(t) = e^{-i\omega t}a(0),\ a^\dagger(t) = e^{i\omega t}a^\dagger(0). \tag{3.9}$$

From this it follows

$$\phi_a = \sqrt{\frac{\hbar Z}{2}}(e^{-i\omega t}a + e^{+i\omega t}a^\dagger), \tag{3.10}$$

$$q_a = \sqrt{\frac{\hbar}{2Z}}i(e^{+i\omega t}a^\dagger - e^{-i\omega t}a). \tag{3.11}$$

If we remember the definition of impedance, we see that the equivalent terms in ϕ and q, that is those that rotate at the same frequency, are proportional to each other by a factor Z

$$\frac{\tilde{\phi}_a(+\omega)}{\tilde{q}_a(+\omega)} \sim \frac{\tilde{V}_a(+\omega)}{\tilde{I}_a(+\omega)} \sim -iZ. \tag{3.12}$$

It also follows that the flux-charge or voltage-current variables form elliptical orbits in phase space, which are traversed with a frequency ω

$$\phi_a(t) = \cos(\omega t)\phi_a(0) + \sin(\omega t)Zq_a(0), \tag{3.13}$$

$$q_a(t) = \cos(\omega t)q_a(0) + \sin(\omega t)\frac{1}{Z}\phi_a(0). \tag{3.14}$$

3.3 Transmission lines or waveguides

So far we have seen that the superconductor admits linear excitations that combine charge, currents and a confined electromagnetic field, and that these microwave excitations behave like photons in a box or in a cavity. We are now going to study circuits that allow the photons to move freely, introducing the notion of propagating photons and continuous fields.

The are various elements that can potentially conduct microwaves and a allow the guided transport of photons. The simplest one would be just a coaxial cable, such as the ones that bring the TV signal to our receivers. These cables consist of a conducting core and a conducting shell around it, separated by some dielectric. The electromagnetic waves move longitudinally in the free space among metals, carrying with them charge and current excitations on the surface of both conductors.

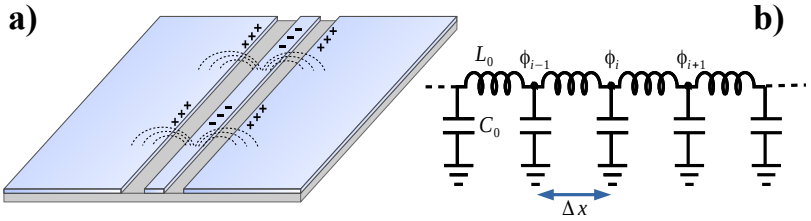

Figure 3.2: (a) Picture of a coplanar waveguide. The left and right superconducting planes are grounded to a fixed potential while the charge and electromagnetic waves run through the middle section. (b) Reminder of the equivalent circuit.

The equivalent device in a 2D superconducting microchip would be either a stripline or a coplanar waveguide. The former consists on two strips of superconducting material, one sitting above and one below the substrate. The field moves in between both lines, confined in the substrate. The coplanar waveguide, on the other hand, consists on a thin superconducting line surrounded by larger planes that are connected to ground or some fixed potential. Now the electromagnetic field runs outside and inside the substrate, and this, together with the larger size of the ground planes seems to isolate better the propagating waves from external disturbances.

From a physical point of view, any of these devices behaves like a one-dimensional circuit with has some inductive and capacitive energy distributed along it. The capacitive energy arises from the interaction between the core conductor and the ground plates, while the inductive energy arises from the natural resistance of the material to changes in the current — a kind of intrinsic "inertia". Mathematically, we model these two ingredients by discretizing the waveguide into a series of small inductors and capacitors, connected as in figure 3.2b.

We are now going to proceed to the quantization of that model, starting from the Hamiltonian that was already derived in §2.2.2. This will be done in two different setups, open and periodic boundary conditions. The reason is simple: while microwave cavities made of "open" cables with endings will be best described by open boundary conditions, the eigenmodes of that problem correspond to standing waves. It is therefore more convenient, once we move to studying propagating

photons, to have a problem with eigenmodes that carry a well defined momentum, and where moving wavepackets can be defined.

3.3.1 Periodic boundary conditions

Let us assume a fictitious coplanar waveguide that closes on itself. The Hamiltonian that describes the equivalent discretized circuit is (2.18), which may be written

$$H = \sum_{i=1}^{N} \frac{1}{2C_0} q_i^2 + \sum_{i=1}^{N} \frac{1}{L_0} (\phi_{i+1}^2 - \phi_{i+1}\phi_i). \tag{3.15}$$

The electric properties of each segment $\Delta x = d/N$ are proportional to the capacitance and inductance densities, $C_0 = c_0 \Delta x$ and $L_0 = l_0 \Delta x$.

The second term in this model is a quadratic form, $\frac{1}{2L_0}\phi^T B \phi$, with a non-negative, symmetric matrix B that is of the form introduced in §A.3. The Hamiltonian can be diagonalized following the prescriptions from §A.4. We modify this procedure slightly in order to introduce some length scale in the problem. For that we assign positions $x_m = \Delta x \times m$ to each segment, and obtain the quasimomenta

$$k = \frac{2\pi}{d} \times n \in \left(-\frac{\pi}{\Delta x}, \frac{\pi}{\Delta x}\right], \tag{3.16}$$

where d is the total length of the cable. The result is an expansion in terms of creation and anihilation operators

$$\begin{aligned} \phi(x_m) &= \sum_k \sqrt{\frac{\hbar}{2c_0\omega_k}} \left(\frac{e^{ikx_m}}{\sqrt{d}} b_k + \frac{e^{-ikx_m}}{\sqrt{d}} b_k^\dagger \right), \\ q(x_m) &= \Delta x \sum_k \sqrt{\frac{\hbar c_0 \omega_k}{2}} i \left(\frac{e^{ikx_m}}{\sqrt{d}} b_k^\dagger - \frac{e^{-ikx_m}}{\sqrt{d}} b_k \right), \end{aligned} \tag{3.17}$$

The eigenfrequencies of the problem are

$$\omega_k = \frac{1}{\sqrt{C_0 L_0}} \sqrt{2 - 2\cos(k\Delta x)}, \tag{3.18}$$

and for small momenta the dispersion relation is approximately linear

$$\omega_k \simeq c|k|,\ c = \frac{1}{\sqrt{c_0 l_0}},\ |k| \ll \frac{1}{\Delta x}. \tag{3.19}$$

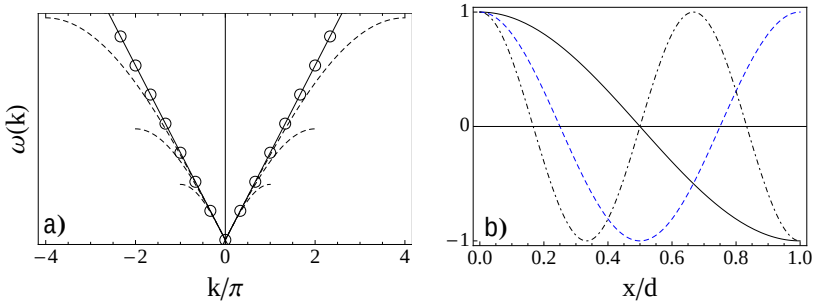

Figure 3.3: (a) Dispersion relations for a transmission line. In dashed line we plot the relations for $\Delta x = 1, 1/2, 1/4$ and in solid line the limiting relation for $\Delta x = 0$. When the transmission line has a finite length $d = 6$, the momenta and frequencies are discrete (circles). (b) First flux modes for an open trasmission line of finite length.

The dispersion relation only depends on intensive properties of the line. This is illustrated in figure 3.3, where we plot how the intervals of allowed photon momenta increases with decreasing Δx, but the whole relation has a well defined limit. The same happens with the definitions of the charge and flux operators, which depend only on intensive quantities, c_0, ω, and normalized modes. This allows us to obtain the continuum limit introducing the charge density operator, $\rho(x) = q(x)/\Delta x$, and the effective low-energy Hamiltonian

$$H = \int_0^d \mathrm{d}x \left\{ \frac{1}{2c_0}\rho(x)^2 + \frac{1}{2l_0}\left[\partial_x \phi(x)\right]^2 \right\}, \tag{3.20}$$

which corresponds to a massless Klein-Gordon theory with periodic boundary conditions $\phi(x + d) = \phi(x)$.

3.3.2 $\lambda/2$ microwave cavities

When the transmission line has a finite length, only a discrete set of microwave frequencies is allowed into the transmission line. If the transmission line is cut, photons are reflected by the ends of the cable, forming standing waves that are our eignmodes, in a very similar way in which photons would be confined by a mirror in a Fabry-Perot cavity.

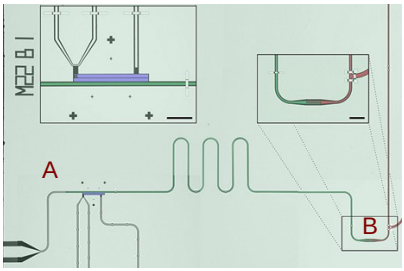

Figure 3.4: A $\lambda/2$ resonator coupled to one qubit and connected via two capacitors (A, B) to input and output ports.

Working in the continuous limit, we can model the reflection of photons through Neumann boundary conditions

$$\partial_x \phi|_{x=0,d} = 0 \tag{3.21}$$

In other words, since the line is cut open, the previous equation states can be no current at the borders. The Hamiltonian of the problem is the same one (3.20), but now it is solved by a different set of modes

$$u^{(n)}(x) = \sqrt{\frac{2}{d}} \cos\left(\frac{\pi n}{d} x\right), \; n \in \mathbb{N} \tag{3.22}$$

where $k_n = \pi n/d$ plays the role of the quasimomentum, even though all modes are standing waves. In figure 3.3a we plot the shape of the first three eigenmodes, which indeed have zero derivative at the edges of the line and span *half a wavelength*.

While a $\lambda/2$ resonator has no current at the edges, its modes reach maximum values of the charge on the edges

$$\rho(x) \quad = \quad \sum_n u^{(n)}(x) \sqrt{\frac{\hbar c_0 \omega}{2}} i \left(b_n^\dagger - b_n\right). \tag{3.23}$$

Thus, if we connect two capacitors to the ends of the line, we will achieve a large electric coupling that allows us to inject and retrieve photons in and out of the cavity. As shown in figure 3.4, a typical design actually builds a $\lambda/2$ resonator from a larger coplanar waveguide or transmission line, that is cleverly interrupted at two points to create two capacitors (the "B" inbox in figure 3.4). The coupling to the

environment can be enhanced by enlarging the capacitor surface and since it all depends in geometric properties of the circuit, it can be very accurately engineered and manufactured.

3.3.3 $\lambda/4$ microwave cavities

Just for the sake of completeness, we have to mention a final type of cavity that consists on a superconducting cable that is connected to ground. Unlike figure 3.4a, one of the edges of this cavity will not be a capacitor, but a direct connection to the ground plane that surrounds the coplanar waveguide. This connection sets a different boundary condition, which is that the voltage on that extreme has to become zero

$$V(d) = \dot{\phi}(d) = 0. \tag{3.24}$$

If we go back to the theory of photon modes, and combine this equation with the boundary condition $\partial_x \phi(0) = 0$, we find that the appropriate modes now read

$$u^{(n)} \propto \cos\left(\frac{\pi n}{2d} x\right). \tag{3.25}$$

Therefore, fundamental mode ($n = 0$) now has a wavelength $\lambda = 4d$, from where the name derives.

These type of cavities are interesting because close to the edge $x = d$ the current is maximal. This will be beneficial when coupling inductively the cavity to other circuits, or when tuning the cavity properties by means of tunable inductances.

3.4 Photon states

The superconducting circuit literature is rich in examples of creation, manipulation and detection of different photon states. One of the pinnacles of this technology is the work by M. Hofheinz [HWA+09], where arbitrary superpositions of up to 15 photons could be engineered and characterized through advanced tomography and Wigner function reconstruction. In the following we summarize just a limited set of states that have been used and which are of interest for the following discussions.

3.4.1 Single mode Fock states

The simplest configurations that can be built mathematically through the creation and anihilation operators are few-photon states. Starting from the vacuum, $|0\rangle$, with no photons, we build all other states

$$|n\rangle = \frac{a^{\dagger\, n}}{\sqrt{n!}} |0\rangle \,. \tag{3.26}$$

Despite the mathematical simplicity of these states, and their utility in protocols for cryptography, quantum computation and quantum simulation, there are important experimental difficulties for their creation:

- **Creation:** A Fock state is typically created by injecting photons one by one into the vacuum. This demands a good source of single photons on demand, which is hard to build.
- **Detection:** Typical electronics measures expectation values of the voltage and current, which are related to the quadratures $\langle a + a^\dagger \rangle$ or $\langle a - a^\dagger \rangle$. They average to zero in these states.
- **Detection:** The only discriminating tool for Fock states is a photon counter. Photon counters can be built either directly or from photodetectors in the visible/IR/UV regime, but they do not exist for microwaves.

3.4.2 Single mode coherent states

The next most familiar state in the line, a coherent state is a superposition of all Fock states, characterized by an average number of photons and a phase

$$|\alpha\rangle = \sum_n \frac{\alpha^n}{\sqrt{n!}} e^{-|\alpha|^2/2} |n\rangle \,, \tag{3.27}$$

$$a\,|\alpha\rangle = \alpha\,|\alpha\rangle \,, \tag{3.28}$$

$$\langle\alpha|\, n\,|\alpha\rangle = |\alpha|^2. \tag{3.29}$$

Coherent states in the visible regime and nearby regions of the spectrum are hard to produce and required the invention of the laser to be generated. Microwave coherent states, on the other hand, may be easily generated by conventional microwave electronics, where the amplitude

and phase can be very precisely tuned in almost real time (picoseconds). Moreover, if we know that we have a coherent state, it is very easy to characterize it, as the expectation values of the two quadratures, $\langle a \pm a^\dagger \rangle$, corresponding to voltage and intensity, provide us with the real and imaginary parts of the coherent state variable α.

3.4.3 Thermal states

At a finite temperature T ($\beta = 1/k_B T$) we expect a Bose-Einstein distribution of particles populating the resonator. This distribution is obtained as

$$\rho = \frac{e^{-\beta H}}{Z(\beta)} = \sum_{n=0}^{\infty} e^{-\beta \hbar \omega n}(1 - e^{-\beta \hbar \omega}) \left|n\right\rangle \left\langle n\right|, \tag{3.30}$$

which results in an average number of photons

$$\langle \hat{n} \rangle = \langle a^\dagger a \rangle = \frac{1}{e^{\hbar\omega/k_B T} - 1}. \tag{3.31}$$

In actual experiments we expect to work with frequencies of ω from 1 to 10 GHz, typically, because that is a comfortable range for convetional electronics. If we recall that $\hbar \times 20\text{GHz} \simeq k_B \times 1\text{K}$, this means that for an experimental range of temperatures from $T \simeq 10\text{mK}$, the average population of photons ranges between 0.006 and 10^{-44}. In other words, from all practical points of view, for this range of frequencies cavities and lines can be assumed to be very close to a perfect vacuum.

Can we "engineer" thermal states? Having a resistive element in the circuit will amount to having a thermal environment with which the line may interact and, if this element is not too close to our chip, one can conceivably warm it with suitable currents to generate thermal radiation. If we do not want to warm up the resistance and thus the chip, we can inject that radiation from outside the experiment, much like ordinary fields are injected to control qubits and lines.

3.4.4 Gaussian states

Coherent states and thermal states are two representatives of a larger family of states, the so called Gaussian states [WPGP+12], which have the property that they can be characterized by the first and second

moments of the Fock operators, $\{\langle a_n \rangle, \langle a_n^\dagger \rangle, \langle a_n^\dagger a_m \rangle, \langle a_n a_m \rangle\}$, with all other expectation values being derived through Wick's theorem.

As in the case of coherent states, Gaussian states have the advantage that they can be created through linear transformations or quadratic Hamiltonians (i.e. Hamiltonians that only contain up to even powers of charge and flux, and no nonlinearities) starting from coherent states. Moreover, they can also be fully understood through the measurement of first and second order moments, a feat that is possible with current electronics.

From a mathematical point of view, Gaussian states are also convenient because their entanglement properties can be fully obtained from the covariance matrix. If we introduce a vector of position and momenta,

$$q_n = b_n + b_n^\dagger,\ p_n = i(b_n^\dagger - b_n), \tag{3.32}$$

and join them in a single vector, $\mathbf{x} = (q_1, p_1, \ldots, q_N, p_N)$, the state is fully determined by the first moment $\bar{\mathbf{x}}$ and the covariance matrix, γ,

$$\bar{\mathbf{x}} = \langle \mathbf{x} \rangle = \mathrm{Tr}(\mathbf{x}\rho), \tag{3.33}$$

$$\gamma_{ij} = \frac{1}{2} \langle x_i x_j + x_j x_i \rangle - \langle x_i \rangle \langle x_j \rangle . \tag{3.34}$$

3.4.5 Two-mode squeezed states

The two-mode squeezed state is a particular instance of a Gaussian state with two bosonic modes that are entangled [LKOH+05]. In order to have entanglement between two modes, these have to interact for a period of time. We can extract the entangling part of the evolution into a unitary that involves both modes

$$U = \exp\left[\frac{1}{2}(\epsilon b_j^\dagger b_i^\dagger - \epsilon^* b_i b_j)\right], \tag{3.35}$$

where $\epsilon = re^{i2\varphi}$ parameterizes the amount, r, and the phase of the squeezing.

A particular example of this state is the two-mode squeezed thermal state, which arises from applying a squeezing operation onto a state with n_1 and n_2 photons on each mode

$$\rho(n_1, n_2, \epsilon) = U(\epsilon)(\rho_{n_1} \otimes \rho_{n_2})U(\epsilon)^\dagger. \tag{3.36}$$

This state is characterized by a particular form of the covariance matrix which, up to simplectic local transformations reads

$$\gamma_{2sq} = \begin{pmatrix} a & 0 & c & 0 \\ 0 & a & 0 & -c \\ c & 0 & b & 0 \\ 0 & -c & 0 & b \end{pmatrix}, \tag{3.37}$$

with the parameters ($\varphi = 0$)

$$a = n_1 \cosh(r)^2 + n_2 \sinh(r)^2 + \frac{1}{2}\cosh(2r) \tag{3.38}$$

$$b = n_2 \cosh(r)^2 + n_1 \sinh(r)^2 + \frac{1}{2}\cosh(2r) \tag{3.39}$$

$$c = (n_1 + n_2 + 1)\frac{1}{2}\sinh(2r). \tag{3.40}$$

Instead of studying how states are transformed by this operation, we can study its effect on the observables. This is given by the transformation

$$c_1 = \mu b_1 + \nu b_2^\dagger \ (= U b_1 U\dagger), \tag{3.41}$$

$$c_2 = \mu b_2 + \nu b_1^\dagger, \tag{3.42}$$

with the squeezing parameters $\mu = \cosh(r)$ and $\nu = e^{i\varphi}\sinh(r)$. The mixing of modes is a form of correlation that can make the quantum uncertainty of a linear combination of the two modes be smaller than that of the individual modes. More precisely, introducing the observables

$$x_\pm(\phi) = \frac{1}{2\sqrt{2}}(b_1 + b_2)e^{i\phi} + \text{H.c.}, \tag{3.43}$$

and assuming that the squeezing acts on the vacuum state, we find that the variance of this operator is

$$\Delta x_\pm(\phi) = \frac{1}{4}[\cosh(2r) - \sinh(2r)\sin(\phi - \varphi)]. \tag{3.44}$$

The maxima and minima of this are $\frac{1}{4}e^{\pm 2r}$, and are, respectively, smaller and larger than $\Delta x_i = 1/4$.

3.4.6 Transmission line vacuum state

We close this section by studying the ground state of a transmission line. As in the case of the LC resonator, the lowest energy state is obtained by setting all modes to a vacuum. In other words the line vacuum

$$|\Omega\rangle = \bigotimes_k |0_k\rangle \tag{3.45}$$

and it satisfies $b_k |\Omega\rangle = 0$ for all modes.

Note however that the ground state condition is set in frequency or momentum space, the space of quantum numbers that characterize the different photon states. In real space, the field operators $\phi(x)$ and $\rho(x)$ do not have well defined values and $|\Omega\rangle$ is not even an eigenstate of these operators. This is obvious when inspecting the mode expansion (3.17), where the operators ρ and q are shown to be linear combinations of b_n and $b_n^\dagger$.

There are however deeper implications of the vacuum structure. The Hamiltonian that describes the line arises from a chain of coupled oscillators and this coupling is capable of correlating distant points, creating entanglement already in this seemingling innocent state. Equation (3.17) also supports this point. If we compute the correlation between flux operators we obtain

$$\langle \phi(x)\phi(y)\rangle - \langle \phi(x)\rangle \langle \phi(y)\rangle = \sum_k \frac{\hbar e^{ik(x-y)}}{2c_0 \Delta x \omega_k} \langle b_k b_k^\dagger \rangle \,, \tag{3.46}$$

an expression divergent both in the infrared and ultraviolet limit[1] The effect of these vacuum fluctuations between different points in time and space in the 1D line can be used to probe deep results from quantum field theory and causality.

3.5 Control of photons

3.5.1 Enegy injection

We start by considering how to insert energy in and out of the microwave resonators, moving them away from their equilibrium configu-

[1]Infrared because the denominator approaches zero for $k = 0$, and ultraviolet because the fraction is proportional to $1/n$ for $|n| = 1, \ldots, N/2$ and the sum diverges logarithmically with the discretization size.

ration, which is the vacuum state. Normally we will have a setup like the one in figure 3.4, where the transmission line forms a cavity and is prolongued, through a capacitor [Node B] to a line that connects with some signal generators and detectors.

The Hamiltonian that describes this configuration reads more or less as follows

$$H = \hbar\omega a^\dagger a + \hbar(\Omega^*(t)a + \Omega(t)a^\dagger), \tag{3.47}$$

where $\hbar\omega$ is the mode that interests us and $\Omega(t)$ is groups the external field times the coupling to the antenna that feeds the cavity.

There are two possibilities to the previous model. If Ω is a static field, the Hamiltonian can be diagonalized by displacing the field operators $a \to a + \Omega/\omega$. This implies that the ground state is now a displaced vacuum state, a coherent state with ampliude $|\Omega/\omega\rangle$.

The static field approach can be quite inefficient, as we need large coupling strengths or large field amplitudes. If our cavity is weakly coupled to the environment, so as to increase the lifetime of photons, then $|\Omega/\omega| \ll 1$. In this case it is more convenient to use a resonant time-dependent driving, $\Omega(t) \simeq \Omega_0 \exp(-i\omega t)$. Moving to a rotating frame, we can write the actual state $|\psi\rangle = \exp(-i\omega t)\,|\xi\rangle$, where the state ξ evolves with the Hamiltonian $H_{eff} = \Omega_0 a^\dagger + \Omega_0^* a$. After a time t, the resulting state is again a displaced vacuum, but the displacement is arbitrarily large, $|\Omega_0 t\rangle$.

3.5.2 Losses

The same way that energy may creep into the resonator through antennas, it may also leak out. A proper model for the cavity is given by the master equation [cf. §A.5]

$$\partial_t \rho = -i[\Omega_0 a^\dagger + \Omega_0^* a, \rho] + \frac{\kappa}{2}(2a\rho a^\dagger - a^\dagger a\rho - \rho a^\dagger a). \tag{3.48}$$

The losses rate κ, as mentioned before, is related to the coupling with the outgoing transmission line and the density of states in the line at the frequency of the cavity, ω. Experiments typically make this rate κ small, around MHz, so that leakage of photons from the cavity is the slowest process in the experiment. Under these conditions the relative linewidth of the cavity will be very small, leading to a large quality

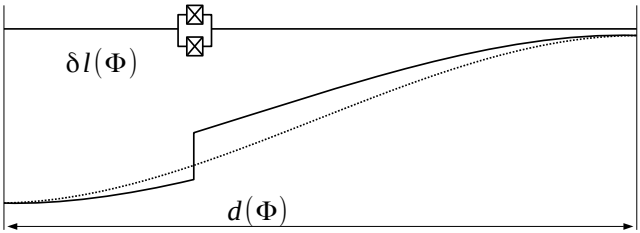

Figure 3.5: A $\lambda/2$ resonator with a SQUID becomes akin to a tunable cavity. The localized inductance due to the SQUID depends on the external flux; it behaves as an additional length added to the cavity. In solid and dashed we plot the modes with and without the perturbation induced by the SQUID.

factor, $Q = \omega/\kappa$, which can be as large as 10^6 –one million oscillations of the photon before it is lost!

The losses of the cavity have also another side effect: when applying the resonant driving Ω_0 above, the cavity vacuum is no longer displaced to arbitrarily large values. Instead the displacement of the field evolves as

$$\frac{d}{dt}\langle a\rangle = -i\Omega_0 - \frac{\kappa}{2}\langle a\rangle\,, \tag{3.49}$$

which converges to

$$\langle a\rangle\,(t\to\infty) = \frac{2i\Omega_0}{\kappa}. \tag{3.50}$$

3.5.3 Cavity tuning

Superconducting resonators have an attractive feature that in the optical regime is harder to achieve: the resonator frequency can be tuned by a rather large amount, both statically and in a time-dependent fashion. The trick is achieved by means of a circuit that was studied in 2.2.5. A parallel combination of identical Josephson junctions behaves as a small circuit with an inductance that is proportional to the flux: more precisely, $1/\delta L \propto 4E_J\cos(\Phi_0/2\varphi_0)$. This localized change of inductance is like a localized change of the speed of light or index of refraction for visible light, resulting in a change of the optical length of the cavity.

This way of tuning microwave cavities has an important advantage over optical cavities; namely, the frequency of the cavity can be tuned

faster than the frequency of the photons themselves [SWP+08]. This allows simulating physical processes in which the mirrors of a cavity move at a speed close to the speed of light, what is known as the Casimir effect [WJP+11]. But even below this regime, modulating the frequency of the cavity can also be used to implement other devices, such as parametric amplifiers and photon entanglers.

Chapter 4

Superconducting qubits

4.1 Introduction

The term *qubit* stems from the combination of words *quantum* and *bit* and denotes a physical system where a two-dimensional Hilbert space can be embedded and faithfully represented and manipulated. In plain words, this means that we can control the system not only to be in one of two orthogonal states, which we label $|0\rangle$ and $|1\rangle$, but in any superposition with arbitrary coefficients, $\alpha|0\rangle + \beta|1\rangle$, that are complex, $\alpha, \beta \in \mathbb{C}$ and properly normalized, $|\alpha|^2 + |\beta|^2 = 1$.

The quantum bit is the basic unit of quantum information and it is also the building block of other devices, such as cryptographic protocols, quantum algorithms and computers or quantum memories. A quantum computer is nothing but a device that is capable of implementing arbitrary unitary transformations on a set of quantum bits, as well as preparing and measuring their individual state. In order to perform this, we need a set of ingredients that are put forward in DiVincenzo's list of requirements for a quantum computer [DiV95]

1. Perfectly distinguishable quantum bits.
   Ideally this implies a physical system with two states. In practice we typically use the two lowest energy eigenstates of a physical system, ensuring that transitions to other excited states are suppressed, either because the energy difference to those states is large, or because of some conservation rule that forbid such

transitions.

2. A procedure to set the qubits to a given, zero state.
   Sometimes this is done by ordinary cooling, but it is preferable to have some mechanism (optical pumping, spontaneous emission) to force the qubit to some initial state.

3. An apparatus that measures the state of the qubits in some basis.
   Sometimes this is not a real apparatus, but some mechanism, such as resonance fluorescence, or the action of the qubit on some passing laser beam, that identifies uniquely the state of the qubit.

4. Arbitrary local operations on each qubit

$$U_i(\vec{v}) = \exp(-i\vec{v}\cdot\vec{\sigma})$$

5. At least one universal quantum gate on each pair of qubits
   Examples of such gates are the CNOT and the CPhase

$$U_{ij}^{Phase} = \exp\left[i\frac{\pi}{4}(\sigma_i^z - 1)(\sigma_j^z - 1)\right]$$

   Note that such entangling gates can only be produced by means of some interaction between the qubits.

6. Sufficiently small decoherence or errors during the previous operations, so that error correction may be implemented.

In this section we are going to discuss how points 1-4 of the previous list are implemented using superconducting circuits. The history of superconducting qubits is a rather long one and predates the most recent ideas of quantum information. The notion of a charge qubit is younger than the ideas of a superconducting island, quantum dots or single-electron transistors. In these notes we do not attempt to track that history but rather to provide the most elementary notions needed to understand the state-of-the-art in the field, perhaps with a strong bias towards the most recent designs and developments. Hence, while there are many experiments in superconducting islands or many implementations of flux-based or phase-based qubits, we will focus on those that are most commonly used nowadays.

4.2 Charge qubit

A charge qubit is a simple superconducting island that is connected to a charge reservoir through a tunneling elmement, such as a Josephson junction. This element allows charge to enter and exit the island, and the small size of the island restricts itself, through Coulomb blockade, the amount of excess charge that can populate it.

A picture of such a device is shown in figure 4.1a, together with the equivalent circuit that was already analized in §2.2.3. The novelty in figure 4.1 is two parallel junctions that couple the island to the ground plane, and which enclose a small region through which some magnetic flux is threaded. As it was explained in §2.2.5, the parallel-junction circuit or DC-SQUID behaves in practice as a single junction with a tunable inductance. This means that we can implement the charge-qubit Hamiltonian

$$H = \frac{1}{2C_\Sigma}\left(q - q_g\right)^2 - E_J \cos(\phi/\varphi_0). \tag{4.1}$$

using an equivalent circuit 4.1b where E_J is tunable.

The charge qubit Hamiltonian (4.1) contains a capacitive and an inductive energy. The eigenstates of the first term are the eigenstates of the charge operator

$$q\left|n\right\rangle = 2en\left|n\right\rangle, \quad n \in \mathbb{Z}. \tag{4.2}$$

They are defined in terms of the excess or defect of Cooper pairs, n relative to the neutral configuration, $n = 0$. The energy of each state is therefore

$$E_n = \frac{2e^2}{C_\Sigma}(n - n_g)^2 = 4E_C(n - n_g)^2, \tag{4.3}$$

a function of the charging energy

$$E_C = \frac{e^2}{2C_\Sigma} \tag{4.4}$$

and of an equilibrium charge, n_g, that depends linearly on the external or *gate* potential V in figure 4.1b.

The parabolic dependence of the capacitive energy, together with the gate voltage, are almost sufficient to define a qubit. As shown in figure 4.2, around $n_g = \frac{1}{2}$, the states $|0\rangle$ and $|1\rangle$ are almost degenerate

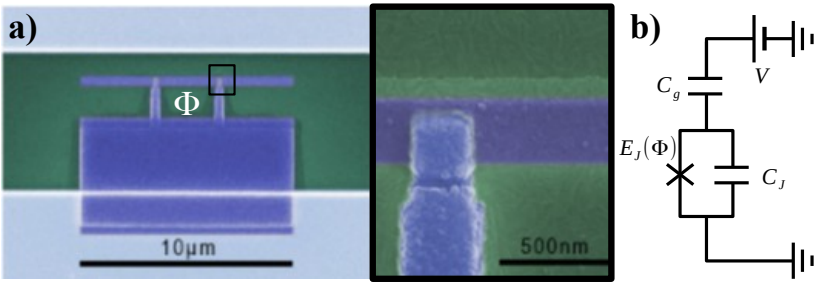

Figure 4.1: (a) Superconducting island coupled to the ground plane through two Josephson junctions, one of which is shown in a zoomed picture. Pictures courtesy of Andreas Wallraff, ETH, Zurich. (b) Reminder of the equivalent circuit discussed in §2.2.3. Note that the two junctions add up to a single effective junction with a variable nonlinear inductance that depends on the flux Φ enclosed by the loop.

and well separated from all other charge states. This makes it possible to experimentally distinguish those states and, hopefully, to also address and induce transitions among them.

However, to induce such transitions we need need an element that may change the number of Cooper pairs, introducing *quantum fluctuations*. In our model this is achieved by the Josephson junction, which allows pairs to tunnel in and out of the superconducting island, and whose nonlinear energy functional admits a simple representation in the number basis describing those hopping processes §A.1

$$\cos(\phi/\varphi_0) = \frac{1}{2}\sum_n \left(|n+1\rangle\langle n| + |n\rangle\langle n+1|\right). \tag{4.5}$$

If we restrict ourselves to the lowest energy levels $|0\rangle$ and $|1\rangle$, we can write an effective Hamiltonian that includes deviations from the degeneracy point and the minimum energy gap, Δ,

$$\epsilon = 8E_C\left(n_g - \frac{1}{2}\right), \tag{4.6}$$

$$\Delta = E_J(\Phi), \tag{4.7}$$

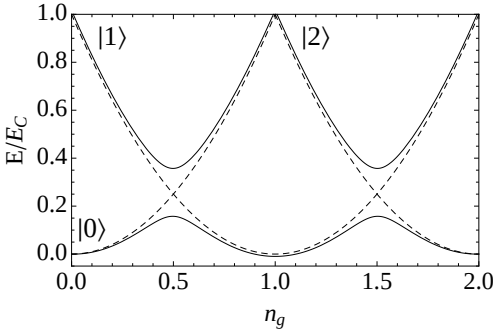

Figure 4.2: Energy levels of the charge qubit without Josephson junction (dashed) and with the tunnelling amplitude $E_J \simeq 0.1E_C$ (solid). At zero voltage the lowest eigenstates are $|0\rangle$ and $|1\rangle$. At $n_g = 1/2$, both states become almost degenerate but the tunnelling create new eigenstates that are superpositions of the former $|\pm\rangle = \frac{1}{\sqrt{2}}(|0\rangle \pm |1\rangle)$..

obtaining the model

$$H = \frac{\epsilon}{2}\sigma^z + \frac{\Delta}{2}\sigma^x. \tag{4.8}$$

Here the flip operator $\sigma^x = |1\rangle\langle 0| + |0\rangle\langle 1|$ replaces the $\cos(\phi/\varphi_0)$ tunneling term and $\sigma^z = |1\rangle\langle 1| - |0\rangle\langle 0|$ does the same with the energy shift induced by the external potential, n_g.

The degeneracy of states 0 and 1 is broken at the symmetry or *degeneracy point*, $\epsilon = 0$. At this point, the true eigenstates are the superposition $|\pm\rangle \propto |0\rangle \pm |1\rangle$, the $|-\rangle$ being the ground state. We can control the gap between these states, $E_J(\Phi)$, through the external flux, and we can move away from the symmetry point $\epsilon = 0$ by applying an external potential. This so called degeneracy point or $\epsilon = 0$ is an important operation point, because the energy gap of the qubit eigenstates,

$$\Delta E = \sqrt{\epsilon^2 + \Delta^2} \simeq \mathcal{O}(\epsilon^2) \tag{4.9}$$

depends only quadratically in ϵ around the symmetry point. In other words, fluctuations of the electromagnetic field applied onto the charge qubit only enter to second order in this formula

$$\Delta E(\epsilon_{noise}) = \Delta E(\epsilon = 0) + \frac{1}{2\Delta}\epsilon_{noise}^2 + \dots \tag{4.10}$$

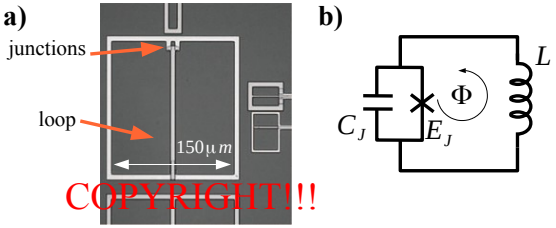

Figure 4.3: (a) Photograph of an RF-squid with two loops, sitting close to a DC-squid which is used for readout. (b) Equivalent circuit of the RF-squid. Picture (a) extracted from [BLP+07].

This is an important realization that allowed experiments with charge qubits to improve significantly their operation time, by keeping the qubit as close to the degeneracy point as possible while doing nothing with it.

Finally, we must remark that the Hamiltonian (4.8) is complete in the sense that it allows implementing arbitrary unitary operations in the qubit. By switching on an off the σ^z and σ^x term, and composing operators, we can perform any rotation in the qubit space with at most two steps.

4.3 Flux qubit

The charge qubit is defined in terms of eigenstates of the charge operator. The flux qubits are, on the other hand, engineered to have as qubit states two eigenstates of the inductive part of the Hamiltonian. The result is, typically, that states $|0\rangle$ and $|1\rangle$ are associated to two supercurrent states rotating without dissipation along a superconducting loop. In order to establish these supercurrents, we play with the quantisation relation (2.1), tuning the flux that is enclosed in the loop so that frustration induces two or degenerate configurations of the branch fluxes, a situation that typically corresponds with having permanent currents on the loop.

4.3.1 RF-squid qubit

The oldest flux qubit consists on a single junction on one side of a loop. The circuit shown in figure 4.3b shows how the flux enclosed in the loop conditions the joint state of the nonlinear inductor and the linear inductor that shunts it. The Hamiltonian for the RF-squid was deduced in §2.2.4

$$H \simeq \frac{1}{2C_J}q^2 + \frac{1}{2L}\phi^2 + E_J \cos\left[\frac{1}{\varphi_0}(\phi + \Phi)\right]. \tag{4.11}$$

Unlike with the charge qubit, we will now focus on the flux/phase variable, interpreting the previous model as the Hamiltonian for a potential that moves along the coordinate ϕ, with a potential $E_{ind}(\phi)$ formed by the linear and nonlinear inductive elements, and with a kinetic energy where C_J plays the role of a mass.

The resulting landscape is summarised in figure 4.4 for two values of the external flux. When there is no magnetic field passing through the loop, the potential has a single absolute minimum at zero flux, $\phi = 0$. In this case the ground state has no charge and also no currents associated to it. However, if we switch on the external flux and move towards a point of "frustration", that is $\Phi/\varphi_0 = \pi$, then the inductive energy develops two absolute minima sitting inside two potential wells. For large enough quantum fluctuations, which in this case are driven by having a small enough mass C_J, the state of the squid is free to tunnel between the two minima, creating two degenerate ground states that can form a qubit.

The RF-squid has a long history that predates its uses for quantum information processing [CB04]. The circuit itself was designed as a magnetometer [SZ67], and it was later on identified as a qubit candidate due to its well defined eigenstates in the quantum regime. The RF-squid is a qubit that is still used in various groups, including the latest D-Wave designs, where its rather large size is an advantage: stretching the superconducting loops [HBJ+07], a single qubit may overlap with several others, creating interactions that are useful for adiabatic quantum computation. However, the size itself can also be a problem, because the qubit becomes more sensitive to stray magnetic fields and has a shorter lifetime under similar conditions to other qubits.

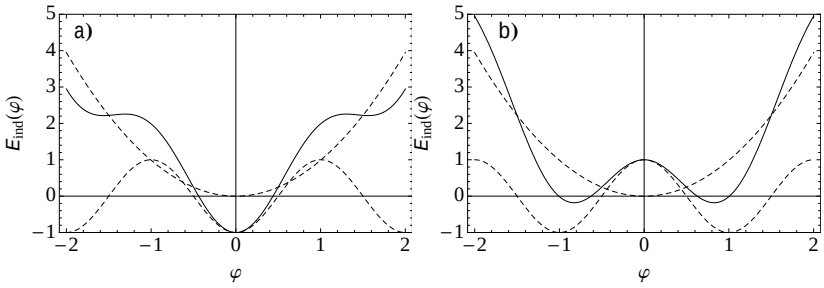

Figure 4.4: Energy levels of the RF-squid for (a) zero external flux and (b) half quantum, $\Phi = \Phi_0/2$. Note that the latter supports two balanced potential wells.

4.3.2 (Three-junction) Flux qubit

The flux qubit based on three (or four junctions) is a more modern design that is currently then one understood when one talks about a "flux qubit". Introduced in [MOL+99] and experimentally demonstrated in [vdWtHW+00], the persistent current flux qubit consists of several Josephson junctions that are serially connected forming a loop, as shown in figure 4.5a. Threading the loop with a magnetic flux we once more achieve frustration and a degenerate ground state whose degeneracy is only broken by quantum fluctuations. The advantage, though, is that now the multiwell structure is achieved only through Josephson junctions, without additional inductors, and it may therefore be much smaller (of a few micrometer size, to be compared with figure 4.3).

The circuit associated to the persistent current flux qubit was already derived in §2.2.6. The effective Hamiltonian has the form

$$H = \frac{1}{2(1/2+\alpha)C_J} q_+^2 + \frac{1}{2C_J} q_-^2 + E_J V(\phi_-, \phi_+) \tag{4.12}$$

with a nonlinear potential

$$V(\phi_-, \phi_+) = \alpha E_J \cos\left(\frac{\Phi - \phi_+}{\varphi_0}\right) - 2E_J \cos\left(\frac{\phi_+}{2\varphi_0}\right) \cos\left(\frac{\phi_-}{2\varphi_0}\right), \tag{4.13}$$

that combines sinusoidal functions with different periodicity, with a shape shown in figure 4.6.

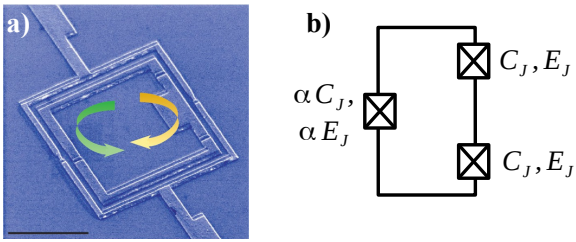

Figure 4.5: (a) Three junction flux qubit, reproduced from [CW08]. (b) Equivalent circuit of the RF-squid. Picture (a) extracted from [BLP+07].

For a fixed external flux Φ, the minimal energy of the nonlinear potential is achieved for $\phi_1 = \phi_2$ or $\phi_- = 0$, because it is at this point that the second term in V is minimal. Note how the interplay between the cosine term that contains Φ, which is rapidly oscillating and has minima at $\phi_+ = \Phi + n\pi\varphi_0$, and the confining $\cos(\phi_+/2\varphi_0)$, which achieves a minimum at $\phi_+ = 0$. As shown in figure 4.6d, for an external flux $\Phi/\varphi_0 = \pi$, the total potential develops two potential minima that are identical and shallow enough to allow tunneling between them.

It is not very hard to diagonalize the Hamiltonian for the 3-junction flux qubit using the number basis. In the regime in which the two potential wells are degenerate, $\Phi/\varphi_0 \simeq \pi$, the two lowest energy states of the Hamiltonian, which we call $|0\rangle$ and $|1\rangle$[1] may become close together and separated from the rest of the spectrum [cf. Figure 4.7a]. This only happens for a limited range of sizes of the small junction, $\alpha \in (0.6, 1.0)$. As shown in figure 4.7b, if the third junction is too small, the third energy level may end up too close to the first level, that is $E_2 - E_1 \simeq E_1 - E_0$. This is not desirable, because if this happens we cannot excite transitions between levels $|0\rangle$ and $|1\rangle$ without having some leakage to level $|2\rangle$ and higher. In other words, we no longer have a functional qubit.

Despite the appearance that the gap to the rest of the spectrum, $E_2 - E_{0,1}$ grows arbitrarily with α, it is also not desirable to have a large α. To understand this we have to write down the Hamiltonian of

[1]Note that here the "0" and "1" are just labels and do not relate to the number of Cooper pairs

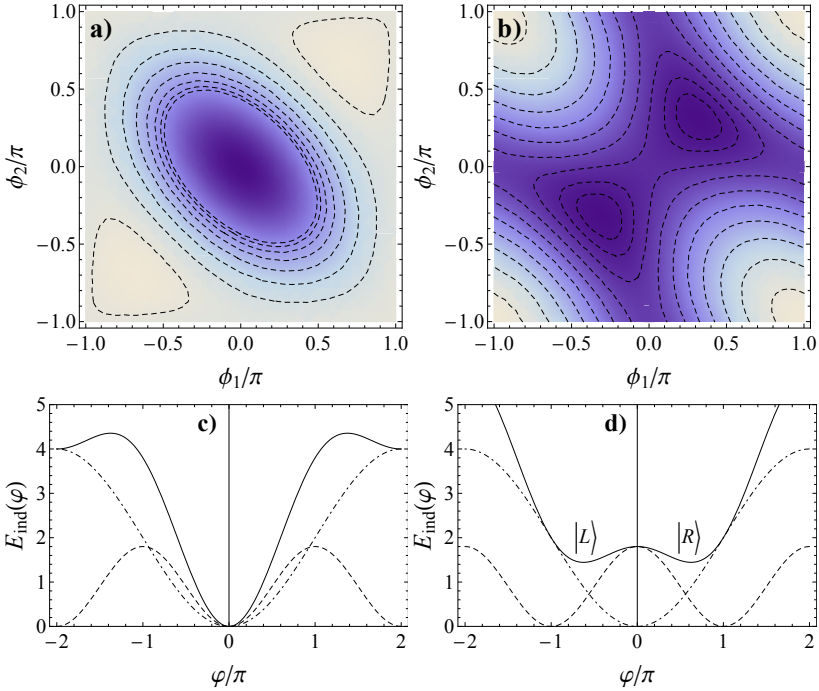

Figure 4.6: Nonlinear inductive potential (4.13) with (a) $\alpha = 0.9$ and no external flux and with (b) $\alpha = 0.9$ and $\Phi/\varphi_0 = \pi$, together with the respective cuts along $\phi_1 = \phi_2 = \varphi_0 \times \varphi$ (c-d).

the flux qubit around the degeneracy point $\Phi = \pi\varphi_0$. Introducing the external flux shift and tunneling gap

$$\epsilon \propto \Phi - \pi\varphi_0 \tag{4.14}$$

$$\Delta = E_1 - E_0, \tag{4.15}$$

and defining the basis states $|L\rangle$ and $|R\rangle$, we recover the same Hamiltonian as in the charge-qubit case (4.8). This has two consequences: first of all, if $\alpha \geq 1$ and the gap Δ becomes almost zero, we lose one of the two operators in H that we need to generate all the unitary rotations of a qubit. Second, if Δ is very small, the sensitivity of the qubit to fluctuations of the magnetic field, increases. Thus, as in the case of the

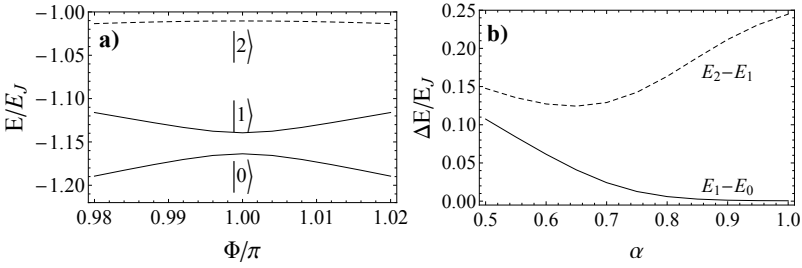

Figure 4.7: (a) Energy levels of the 3-junction flux qubit with anisotropy $\alpha = 0.7$. (b) Energy gap between the "qubit" states $E_1 - E_0$ and also between the first and second excited states, $E_2 - E_1$, as a function of the anisotropy, for $\Phi = \pi\varphi_0$.

charge qubit, it is important to keep as close to the degeneracy point as possible.

Finally, note that the actual eigenstates of the qubit are superpositions of supercurrents rotating clock- and anti-clockwise ($|R\rangle$ and $|L\rangle$, respectively). This is qualitative different from the charge qubit, where the difference was only in a single particle, an extra Cooper pair that enters of leaves the island. In the flux qubit, on the other hand, there exists a current that involves a macroscopic number of pairs with different states depending on the energy and applied flux [vdWtHW+00].

4.4 Transmon qubit

Initial experiments with charge qubits revealed their sensitivity to electromagnetic field fluctuations and charge noise, leading to very low lifetimes. This situation was improved in the seminal work by Wallraff and coworkers [WSB+04], where the Purcell effect was used to enhance both the coupling to the electromagnetic field and the qubit lifetime[2]. Under the conditions of relative isolation provided by the cavity, operat-

[2]The Purcell effect is an enhancement of the coupling of a few-level atom to a few selected frequencies. This enhancement decreases the relative importance of other decay channels and noise. In the optical regime the Purcell effect is achieved by creating either Fabry-Perot cavities from pairs of mirrors, or through whispering gallery modes. In circuit-QED this is done using LC-resonators and microwave cavities, as explained later §6.

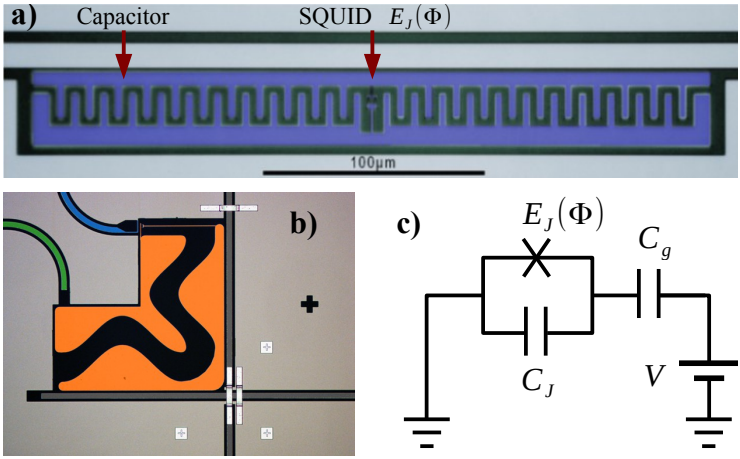

Figure 4.8: (a) Fotograph of a transmon qubit. It consists of a pair of Josephson junctions formin a DC-SQUID configuration, shunted by a large capacitor with interdigitated fingers. (b) Also a transmon, but a different design and location of the junction. (c) Reminder of the equivalent circuit. Fotographs courtesy of Andreas Wallraff, ETH, Zurich.

ing the qubit close to the symmetry point helped in achieving lifetimes of $\gamma_1/2\pi = 0.7$MHz or 1.4μs, a very reduced spontaneous emission rate but with a very short dephasing time.

In 2007 the Yale group realized that the coupling to the environment could be decreased while still preserving the anharmonicity of the circuit [KYG+07]. If we have a look at the charge qubit Hamiltonian

$$H \simeq \frac{1}{2C_\Sigma} q^2 - \frac{C_g}{C_\Sigma^2} qV + \frac{1}{2}\frac{E_J}{\varphi_0^2}\phi^2 - + \frac{1}{2}\frac{E_J}{\varphi_0^4}\phi^4 \tag{4.16}$$

the charge qubit can be seen as a harmonic oscillator, with an anharmonic term that is proportional to E_J and a coupling to the environment that is inversely proportional to C_Σ. Thereby, decreasing the ratio E_C/E_J would amount to decreasing the relative strength of the coupling to the environment, without compromising too much the anharmonicity[3].

[3]Understood as the separation of the qubit states from the upper energy states

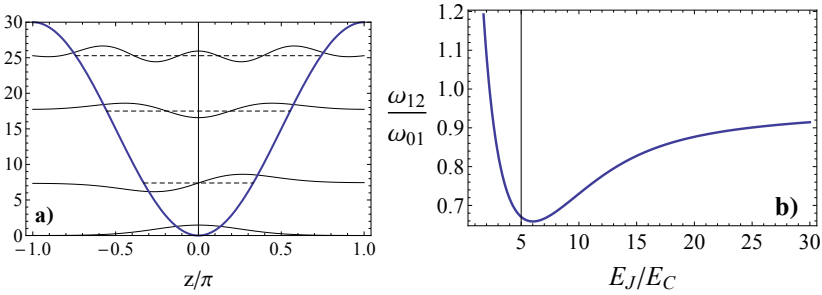

Figure 4.9: (a) Energy levels of a transmon qubit with $E_J/E_C = 15$, plotted together with the originating potential $E_J \cos(\varphi)$. (b) Associated eigenfunctions.

The result of this idea is shown in figure 4.9a-b, and consists of a large capacitor that shunts a Josephson junction. The equivalent circuit is the same as that of the charge qubit. Moreover, the coupling to the microwave photons happens mainly through the electric dipole moment of the qubit, as in the superconducting island. However, the large capacitance, acting as an increased effective mass of the qubit induces the desired effect and the dephasing time grows one order of magnitude with respect to the original experiments [SHK+08]. Since then, it has become possible to improve the quality and even increase the size of transmon qubits, working with 3D setups to achieve lifetimes of the order of 0.1ms. The simplicity of the design and the reproducibility of the qubit properties, with less than 5% fluctuations due to fabrication errors, makes this one of the most used qubits in nowadays experiments.

Using the tools from appendix §A.2 it is possible to compute the eigenenergies of the transmon qubit for different ratios of E_J/E_C. In figure 4.9 we plot the energy levels and the even and odd eigenfunctions corresponding to those energies for a ratio $E_J/E_C = 15$, which is close to the typical experimental values and has been chose only to make the representation more clear. As explained in [KYG+07], the effect of $1/f$ charge noise decreases exponentially with the ratio E_J/E_C, but this comes at a price: increasing E_J/E_C causes the energy level to be less and less anharmonic. As shown in figure 4.9b, the energy difference between the second and third levels, $\omega_{12} = E_2 - E_1$ becomes very similar to ω_{01}. This means that it becomes experimentally hard to

excite transitions between the qubit levels without inducing additional transitions to at least the second state. There is thus a compromise between the experimental ability to address different transitions and the need to decrease charge noise.

Typical experimental values for a 2D transmon (one fabricated on a chip) move around a ratio $E_J/E_C \simeq 50$, with qubit frequencies $\omega_{01} \simeq 6-8$ GHz, and a difference $\delta\omega = \omega_{01} - \omega_{12} \simeq 400$ MHz, which is quite large and can be experimentally resolved with current electronics. The anharmonicity $\delta\omega$ sets also a limit in the speed at which the qubit can be manipulated: if we send microwave pulses that are shorter than $2\pi/\delta\omega$, the pulse will be broader than $\delta\omega$ in frequency spectrum, being able to excite both the $|0\rangle \to |1\rangle$ and the $|1\rangle \to |2\rangle$ transition.

An added value of the transmon, besides its good qubit properties, is the fact that we have extra levels to manipulate, store information and do quantum operations. There are many experiments where the transmon is no longer operated as a qubit, but as a three-level system (qutrit), profiting from the higher level transitions to induce interactions between photons at frequencies ω_{01} and ω_{12}, the so called cross-Kerr interactions [HKP+13].

4.5 Qubit control

4.5.1 Single-qubit operations

Irrespective of the superconducting qubit we are working with, they all can be reduced, in the the two-level approximation, to an effective Hamiltonian with two control parameters

$$H_{qb} = \frac{\hbar\Delta}{2}\sigma^z + \frac{\hbar\epsilon}{2}\sigma^x. \tag{4.17}$$

At the degeneracy point, $\epsilon = 0$, the qubit gap is minimal and given by the frequency Δ. This is the customary working point for the charge, flux and transmon qubits, as mentioned before. Evolution at this point simply adds phases to the qubit states

$$U(t;\Delta,0) = e^{-i\Delta t/2}\,|0\rangle\langle 0| + e^{i\Delta t/2}\,|1\rangle\langle 1|\,. \tag{4.18}$$

Applying a large and uniform external field we can temporarily change the qubit Hamiltonian into something of the form $\hbar\epsilon_0\sigma^x/2$,

where $\Delta \ll \epsilon_0$ allows us to neglect the gap. Such pulses induce an approximate evolution

$$U(t;0,\epsilon_0) = e^{-i\epsilon_0\sigma^x t/2} = \begin{pmatrix} \cos(\epsilon_0 t/2) & -i\sin(\epsilon_0 t) \\ -i\sin(\epsilon_0 t/2) & \cos(\epsilon_0 t) \end{pmatrix}. \tag{4.19}$$

This unitary operation exchanges population between the $|0\rangle$ and $|1\rangle$ states coherently, rotating the state of the qubit.

In general we do not need to use a very large field to achieve this effect. An alternative is to use a time dependent field

$$\epsilon(t) = \Omega\cos(\omega_0 t + \varphi). \tag{4.20}$$

To analyze this control, we rotate the Hamiltonian on a frame that moves at frequency ω_0, with the unitary $U = \exp(-i\omega_0 t\sigma^z/2)$. The original state can be written $|\psi(t)\rangle = U(t)\,|\xi(t)\rangle$, where ξ evolves with the effective Hamiltonian

$$\begin{aligned} H_{\text{eff}} &= U^\dagger H U - iU^{-1}\dot{U} \\ &= \frac{\hbar(\Delta-\omega_0)}{2} + \frac{\hbar\Omega}{4}\left(e^{i\varphi}\sigma^+ + e^{i2\omega_0 t+i\varphi}\sigma^+ \text{H.c.}\right). \end{aligned} \tag{4.21}$$

The last term evolves with a very fast frequency, $2\omega_0$, and if we tune the drive to become resonant with the two-level transition $\omega_0 = \Delta$, it can be neglected. The overall effect is that, in this rotating frame we achieve an interlevel transition, similar to 4.19. It is not hard to see that for a proper tuning of the laser, $\varphi = -t/\omega_0$, or adiabatically switching on and off the pulses, the combined operation

$$U_{tot} = U(t;\omega_0)^\dagger e^{-iH_{\text{eff}}t}U(t;\omega_0) \simeq U(t;0,\Omega/2). \tag{4.22}$$

4.5.2 Dephasing (T_2)

One of the most basic sources of errors in any qubit is dephasing. From the point of view of states, dephasing is a scrambling of the relative phase between different by which coherences are detroyed. Physically, dephasing may be attributed to a perturbation of the qubit Hamiltonian that randomly changes the energies of the $|0\rangle$ and $|1\rangle$ states, that is $H \to H + \delta_{ext}\sigma^z$. When these fluctuations accumulate in time, the only effect they have shows up in the coherences of the density matrix,

$\rho_{01} = \langle 0| \rho |1\rangle = \rho_{10}^*$, which decay exponentially due to such fluctuations

$$\rho(t) = \begin{pmatrix} \rho_{11} & e^{-t/T_2}\rho_{10} \\ \rho_{01}e^{-t/T_2} & \rho_{00} \end{pmatrix}, \tag{4.23}$$

with a time scale known as T_2 or dephasing time.

To understand why this happens, we have to realize that, due to the randomness of the unknown fluctuating perturbations, the physical state has to be represented as an statistical average over different realizations of that noise. In other words, the qubit state is a density matrix that is transformed in time according to a mathematical operation known as quantum channel or positive map

$$\varepsilon(\rho; t) = \int_{-\pi}^{\pi} e^{i\varphi\sigma^z} \rho e^{-i\varphi\sigma^z} p(\varphi; t) \mathrm{d}\varphi \tag{4.24}$$

In this channel, the initial state ρ is randomly perturbed by the evolution with a random phase, φ, whose distribution $p(\varphi; t)$ changes through time. Typically $p(\varphi; t)$ will be centered around 0 and broaden linearly in time, so that the final state may be described by the effective map

$$\varepsilon(\rho; t) = \frac{1}{2} + \frac{1}{2}\mathrm{tr}(\sigma^z\rho)\sigma^z + \frac{1}{2}e^{-t/T_2}[\mathrm{tr}(\sigma^x\rho)\sigma^x + \mathrm{tr}(\sigma^y\rho)\sigma^y], \tag{4.25}$$

or in a more "visual" form from (4.23). Finally, let us note that dephasing may also be treated, under some limits, using the master equation [§A.5]

$$\frac{d}{dt}\rho = \gamma_2(\sigma^z\rho\sigma^z - \rho), \tag{4.26}$$

where $\gamma_2 = 1/T_2$ is the associated decoherence rate.

Dephasing happens in superconducting circuits due to many different reasons. A very obvious one is the large number of control lines that have to be used to stabilize and measure the states of qubits and cavities. Those lines, and other surrounding controls, may carry fluctuating electromagnetic fields that change the potentials and fluxes experienced by the superconducting qubits, thereby changing the energy levels of the qubit without actually inducing transitions.

Another source of dephasing can be due to electromagnetic charges that are trapped in the substrate on top of which the chip is built. These charges typically behave as two-level systems that fluctuate very

slowly and which, in the best of cases, also modify the electromagnetic environment that is seen by the qubits, both between experiments and also within the same experiment (slow $1/f$ noise).

Dephasing is not a very bad type of noise. If we have good control over the qubit Hamiltonian, this noise can be strongly suppressed through NMR control techniques. The most basic one is the so called spin-echo, in which the state of the qubit is reversed at the middle of the experiment, $|\psi\rangle \to \sigma_x |\psi\rangle$ by using one of the operations from §4.5.1. If the electromagnetic environment of the qubit is not significantly modified in between pulses, the total evolution may be written

$$\rho(\delta t + \delta t) = e^{-i\varphi\delta t}\sigma_x e^{-i\varphi\delta t}\rho(0)e^{i\varphi\delta t}\sigma_x e^{i\varphi\delta t} = \rho(0). \tag{4.27}$$

In practice spin echo is never perfect because the energy level fluctuations do not remain constant throughout the experiment and also because there are other sources of decoherence, but it is quite often possible to extend the lifetime of T_2-limited qubits well beyond the original T_2 time.

4.5.3 Relaxation and heating (T_1)

The worst type of decoherence, short of losing the qubit itself, are relaxation, dissipation or heating. In any of these cases the populations of qubit states, together with their coherences, are destroyed, and the density matrix of our circuit converges to some statistical mixture of $|0\rangle$ and $|1\rangle$. All these process can be treated uniformly through a single master equation

$$\begin{aligned} \frac{d}{dt}\rho &= [n(\Delta)+1]\frac{\gamma}{2}\left(2\sigma^-\rho\sigma^+ - \sigma^+\sigma^-\rho - \rho\sigma^+\sigma^-\right) \\ &= n(\Delta)\frac{\gamma}{2}\left(2\sigma^+\rho\sigma^- - \sigma^-\sigma^+\rho - \rho\sigma^-\sigma^+\right). \end{aligned} \tag{4.28}$$

In this equation, the first line contains processes that map ρ to $|0\rangle\langle 0|$, the so called relaxation or cooling, while the second line contains processes that heat the qubit, $\rho \to |1\rangle\langle 1|$.

If the environment is in a more or less perfect electromagnetic vacuum[4], which at our cryogenic temperatures is approximately true,

[4]Except, of course, for the fluctuating charges and other stray fields that pop up along the experiment.

$n(\Delta) \simeq 0$, and deceoherence is pure relaxation, with an evolution

$$\rho(t) = \begin{pmatrix} \rho_{11}e^{-t/T_1} & e^{-t/2T_1}\rho_{10} \\ \rho_{01}e^{-t/2T_1} & \rho_{00} + (1 - e^{t/T_1})\rho_{11} \end{pmatrix}, \tag{4.29}$$

In this equation there is a typical timescale $T_1 = 1/\gamma$ that is associated to the change in populations, and a longer time scale, known as $T_2 = 2T_1$ which is associated to the loss of coherences –in other words, these processes have an implicit dephasing built-in.

Relaxation has always been a problem for superconducting quantum circuits. Among other things, two-dimensional superconducting circuits, despite their rather dissipation-free nature, are in contact with substrate or with open air, and they can radiate part of their energy to those subsystems, which act as coolants and sources of dissipation. This problem is partially solved when qubits are immersed in microwave cavities. In this situation, the coupling to the cavity modes is orders of magnitude stronger than the coupling to the environment, and dissipation become less relevant. Nowadays, with the advent of 3D microwave cavities, which provide almost perfect isolation for the qubits, it becomes possible to observe qubit lifetimes around 100μs. Assuming qubit operation rates of 100MHz, this is a very long lifetime, that allows for 10.000 operations before losses kick in. And even better lifetimes are expected in the near future.

Chapter 5

1D microwave photonics

In this chapter we study the interaction between superconducting qubits and photons that propagate in an infinite transmission line. This setup mimics a new generation of experiments that study the resonances of the qubit through the transmission and reflection coefficients of the incident photons. It also opens the door to the development of both theory and experiments for 1D photonics in regimes of very strong light-matter interaction, a topic that has interest not only in the superconducting circuit community, but in the larger world of nanophotonics and plasmonics.

5.1 Qubit-line interaction

5.1.1 Spin-boson Hamiltonian

We start introducing a rather conventional interaction between the qubit and the transmission line, assuming the linear limit that was used in earlier chapters. Roughly, we assume that charge and transmon qubits couple capacitively to the line, through some effective gate capacitance, C_g, such that the Hamiltonian acquires a term [cf. §2.2.3]

$$H_{int} = Q\frac{V(x)}{C_g}, \tag{5.1}$$

where $V(x)$ is the voltage induced by the line at the position x of the qubit and Q is the charge operator of the qubit itself.

For flux qubits the coupling is a bit more subtle: a current passing through the line induces a magnetic field that can traverse through the qubit superconducting loop. In doing so, the additional flux changes the qubit energy levels [cf. §4.3.2], shifting it a small amount. We can write the interaction

$$H_{int} = g\mu I(x), \tag{5.2}$$

with the effective magnetic dipole of the qubit, μ, and a Landé factor g that quantifies the mutual inductance between the line and the tiny superconducting loop.

In both cases the coupling is linear and we ignore self-interaction terms. Note that the charge qubit couples to voltage, $V(x) = \partial_t \phi(x)$, while in the flux qubit couples to current, $I(x) = \partial_x \phi(x)/l_0$. This is relevant because when we consider the decomposition of the field in modes (3.17), it leads to similar formal expressions. Recalling that in the Heisenberg picture the flux operator reads

$$\phi(x_m, t) = \sum_k \sqrt{\frac{\hbar}{2c_0\omega_k}} \left(\frac{e^{ikx_m - i\omega t}}{\sqrt{d}} b_k + \text{H.c.} \right), \tag{5.3}$$

and using a linear dispersion relation, $\omega_k = v|k|$, we can write the two couplings in much the same form

$$H_{int} = \sigma^\alpha \sum_k (g_k b_k + g_k^* b_k^\dagger). \tag{5.4}$$

Up to irrelevant phases that distinguish the capacitive from the inductive examples, the couplings scale as

$$g_k \simeq i\sqrt{\frac{\hbar}{2c_0} \times \frac{\omega_k}{d}}. \tag{5.5}$$

If we take together the Hamiltonian of the line, the Hamiltonian of the qubit and their interaction, the result is a model that looks as follows

$$H = \sum_k \hbar\omega_k a_k^\dagger a_k + \frac{\hbar\Delta}{2}\sigma^z + \sum_k \sigma^x (g_k a_k + g_k^* a_k^\dagger). \tag{5.6}$$

This is the so called spin-boson model [LCD+87], a paradigmatic model in the study of dissipative systems, where the bosonic system is normally regarded as a bath or environment into which the two-level system may lose energy and decohere.

5.1.2 Rotating Wave Approximation

In the limit of weak couplings, we can make two approximations. The first one is the so called Rotating Wave Approximation, where we neglect the influence of the counterrotating terms $\sigma^+ a_k^\dagger + \sigma^- a_k$ to the dynamics, assuming that their effect averages out very rapidly. A simple argument for this approximation is that the Fermi golden rule predicts a transition matrix element of order $|g_k/(\omega_k + \Delta)|$ for these terms, which is much smaller than the transition matrix element for the resonant terms, $\sigma^+ a_k + \sigma^- a_k^\dagger$, which is of order $|g_k/(\omega_k - \Delta)|$.

Under the conditions of the RWA we simplify the qubit-line interaction to a generalized Jaynes-Cummings model

$$H = \sum_k \hbar\omega_k a_k^\dagger a_k + \frac{\hbar\Delta}{2}\sigma^z + \sum_k (g_k \sigma^+ a_k + g_k^* a_k^\dagger \sigma^-). \tag{5.7}$$

In this Hamiltonian the only allowed processes involve absorption of a photon by a deexcited qubit or emission of a photon by an excited one. The model therefore conserves the total number of excitations

$$N_e = \sum_k a_k^\dagger a_k + \frac{\sigma^z + 1}{2}, \tag{5.8}$$

and the wavefunctions of the combined system may be substantially simplified when there are only a small number of qubits and photons.

Once we do the RWA, we can still impose that the qubit be a small perturbation that cannot significantly affect the bath. Assuming that the bath remains approximately constant, quickly losing memory of the qubit's history, we can trace out the bosonic degrees of freedom and study the dynamics of the qubit, which evolves according to the master equation [cf. §**??**]

$$\partial_t \rho = -i[H_{qb}, \rho] + \frac{\gamma}{2}(2\sigma^- \rho \sigma^+ - \sigma^+ \sigma^- \rho - \rho \sigma^+ \sigma^-), \tag{5.9}$$

This equation describes the spontaneous emission of the qubit with a decay rate $\gamma = J(\Delta)/2$ that can be traced back to the spectral function[1]

$$J(\omega) = 4\pi \sum_k \frac{|g_k|^2}{\hbar^2} \delta(\omega - \omega_k). \tag{5.10}$$

[1] The definition is chosen for notational consistency with [LCD+87], where the coupling is $\frac{1}{2} q_0 \sigma^x \sum_k C_k x_k$ and $J(\omega) = \frac{\pi}{2} \sum_k \frac{C_k^2}{m\omega_k} \delta(\omega - \omega_k)$.

5.1.3 Ohmic spin-boson model

The utility of the spectral function goes beyond providing the effective decay rate of a few-level system under conditions of Markovianity. Instead, different functional dependencies of $J(\omega)$ characterize different universality classes that have very different behavior. In particular, the problem with a transmission line and a qubit corresponds to the Ohmic limit of the spin boson model, where $J(\omega)$ grows linearly with the frequency:

$$J(\omega) = 2\pi\alpha\omega^1 \tag{5.11}$$

This result is obtained from the expression of the couplings (5.5). In order to simplify the calculations, let us assume that we could take the transmission line and cut it to form a $\lambda/2$ cavity that is resonant with the qubit splitting, Δ

$$\bar{g} = i\sqrt{\frac{\hbar}{2c_0}\frac{\Delta}{\lambda/2}} = i\sqrt{\frac{\hbar}{2c_0}\frac{\Delta^2}{v\pi}}. \tag{5.12}$$

This allows us to express the couplings of any other transmission line with similar properties as

$$g_k = \frac{\bar{g}}{\Delta}\sqrt{\frac{\pi v\omega_k}{d}}. \tag{5.13}$$

From there it follows

$$J(\omega) = 4\pi\sum_k \frac{v\pi}{L}\left(\frac{|\bar{g}|}{\hbar\Delta}\right)^2 \omega_k\delta(\omega-\omega_k). \tag{5.14}$$

Using the fact that the spacing between frequencies is approximately $\mathrm{d}\omega_k = v\mathrm{d}k = 2v\pi/d$, and that for each frequency there are two values of the momentum that match it, we obtain

$$J(\omega) = 4\pi\left(\frac{|\bar{g}|}{\hbar\Delta}\right)^2 \int \omega_k\delta(\omega-\omega_k)\mathrm{d}\omega_k = 4\pi\left(\frac{|\bar{g}|}{\hbar\Delta}\right)^2 \omega, \tag{5.15}$$

concluding that indeed we have the Ohmic spin-boson model with $\alpha = 2(\bar{g}/\hbar\Delta)^2$.

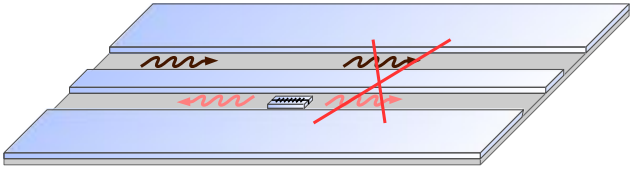

Figure 5.1: An incoming photon is transported by a transmission line towards a superconducting qubit. The qubit, absorbs the photon with some probability, reemitting it, and with some other probability lets is go. The destructive interference between the photon that passes by and the reemitted photon may induce a total reflection of the signal.

5.2 Single photon scattering

In the Rotating Wave Approximation limit, in which the interaction between the qubit and the photons conserves the number of excitations, we can study a particularly simple problem that consists on the interaction between that qubit and a wavepacket that contains a single incoming photon. The formalism to treat this problem differs slightly from the models above, because it is convenient to distinguish left- and right-moving fields on both sides of the qubit [RGRS09, SF05a, SF05b]. This starts by introducing

$$\psi_R(x,t) \propto \sum_{k>0} e^{ikx-ivkt} a_k = \psi_R(x-vt,0), \tag{5.16}$$
$$\psi_L(x,t) \propto \sum_{k>0} e^{-ikx-ivkt} a_k = \psi_L(x+vt,0),$$

which extract the respective right- and left-moving modes and evolve as expected. Ignoring the fact that momenta are cut-off on the negative side, we can still write an effective Hamiltonian

$$\begin{aligned} H &= \int \left[\psi_R^\dagger(x)(-i\hbar v\partial_x)\psi_R(x) + \psi_L^\dagger(x)(+i\hbar v\partial_x)\psi_L(x)\right] \mathrm{d}x \\ &+ \int V\delta(x)\left[\sigma^+\psi_R(x) + \sigma^+\psi_L(x) + \mathrm{H.c.}\right] \mathrm{d}x + \frac{\Delta}{2}\sigma^z. \end{aligned} \tag{5.17}$$

In this model the interaction term amounts also to an approximation by which g_k is approximately constant and independent of the frequency, which is a good approximation for narrow enough wavepackets.

Building on the previous effective model we can solve the dynamics of a state that contains at most one photon, and which is described by the wavefunction

$$|\psi\rangle = \sum_{\alpha=R,L} \int \xi_\alpha(x,t)^* \psi_\alpha(x)^+ |g,0\rangle + e(t)\,|e,0\rangle\,. \tag{5.18}$$

Note how this wavefunction consists of either a qubit in the ground state, $|g\rangle$, with one moving photon, or an excited qubit in a vacuum.

The evolution equations of this problem have a particular form

$$\begin{aligned} i\partial_t \xi_R &= -iv\partial_x \xi_R + \delta(x) V e, & (5.19)\\ i\partial_t \xi_L &= +iv\partial_x \xi_L + \delta(x) V e, & (5.20)\\ i\partial_t e &= \Delta e + V[\xi_R(0) + \xi_L(0)]. & (5.21) \end{aligned}$$

A convenient interpretation of the first two equations shows the existence of a discontinuity in the field, caused by the signal that is injected by the qubit, and which gives rise to the boundary conditions

$$\xi_R(0^+) - \xi_R(0^-) = \frac{V}{iv} e,\ \xi_L(0^+) - \xi_L(0^-) = -\frac{V}{iv} e. \tag{5.22}$$

At this point we are in a position to completely solve the problem. The incident field is assumed to come from the left and is characterized by a signal $a(t) = \xi_R(0^-, t)$ at one side of the qubit, with the physical restriction $\xi_L(0^+, t) = b' = 0$ that no signal is coming form the other side. The output signals are the transmitted and reflected sources, $a'(t) = \xi_R(0^+, t)$ and $b(t) = \xi_L(0^-, t)$, respectively. Under these conditions the qubit dynamics becomes

$$e(t) = -i\frac{V}{\hbar} \int_{-\infty}^{t} e^{-\tilde{\Gamma}(t-\tau)} a(\tau) \mathrm{d}\tau, \tag{5.23}$$

with the effective decay rate $\tilde{\Gamma} = \frac{V^2}{\hbar v} + i\Delta$. All other fields can be extracted from the qubit instantaneous polarization, the incident field and the boundary condition (5.22).

When we study scattering we focus on asymptotic conditions. To do this we can take the limit in which a, b and a' become quasi-static. This can be done by using $a(\tau) = a \exp(-i\omega_{ph} t - \epsilon(t-\tau))$ and taking

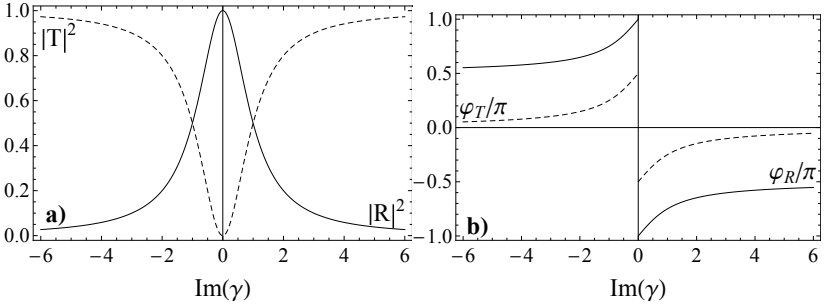

Figure 5.2: (a) Tranmitted and reflected fraction of the photon as a function of the dimensionless parameter $-i\gamma$. (b) Phase slip (in units of π) of the transmitted and reflected photon, φ_T and φ_R, respectively.

the limit $\epsilon \to 0^+$. This leads to a linear relation between scattering coefficients

$$\begin{pmatrix} a' \\ b' \end{pmatrix} = \begin{pmatrix} 1-\frac{1}{\gamma} & -\frac{1}{\gamma} \\ \frac{1}{\gamma} & 1+\frac{1}{\gamma} \end{pmatrix} \begin{pmatrix} a \\ b \end{pmatrix}, \text{ with } \gamma = \frac{\hbar v}{V^2} i\hbar(\Delta - \omega_{ph}), \quad (5.24)$$

defined in terms of the photon frequency ω_{ph}.

The previous linear relation relation leads to the definition of transmission and reflection amplitudes

$$T = \frac{\gamma}{\gamma - 1}, \; R = \frac{1}{\gamma - 1}. \quad (5.25)$$

Note that these coefficients are complex amplitudes. As figure 5.2 shows, the transmitted and reflected intensities are proportional to $|T|^2$ and $|R|^2$, with the consistency relation $|T|^2 + |R|^2 = 1$, while the phase of the coefficients is itself the phase change experienced by those beams. Equation (5.25) and figure 5.2a also show that there is a single resonance at the frequency of the qubit $\omega_{ph} = \Delta$, at which all of the photon is reflected and the qubit acts as a perfect mirror.

5.3 Beyond RWA

So far we have considered a subset of the interaction terms, those that conserve the number of excitations, moving them from the photon space

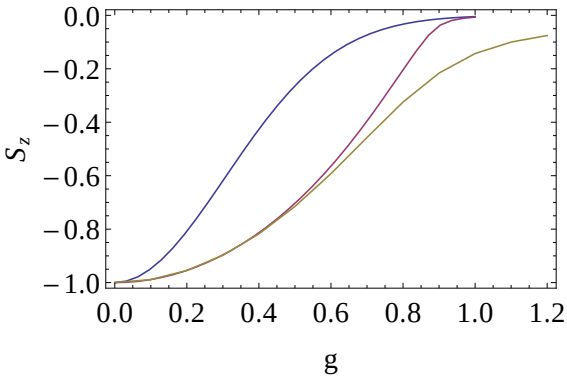

Figure 5.3: Ground state expectation value $S_z = \langle \sigma_z \rangle$ computed with the Lang-Frirsov transformation (blue), a slight variation of it (red) and with Matrix-Product States (yellow).

to the qubit and back. This approximation is justified when the coupling strength is small enough that the ratio $g/(\omega_k + \Delta)$ can be neglected. However, as we will see, when the relative strength of the photon-qubit coupling and the qubit energy is above 10%, this is no longer justified and substantial corrections appear [PZPGR13].

5.3.1 Static properties

The first correction shows up in the static properties of the qubit-line system. While the RWA model (5.7) predicts that the ground state is achieved by a qubit in the vacuum, the full spin boson model contains terms that excite both photons and qubits, invalidating this picture.

A qualitative good approximation to the static properties of the qubit in the line is given by the Lang-Frirsov transformation. This is a unitary transformation that displaces the oscillators based on the qubit state

$$U = \exp[\sigma_x (f_k a_k^\dagger - f_k^* a_k)]. \tag{5.26}$$

More precisely, $U^\dagger a_k U = a_k + f_k \sigma_x$. If we choose $f_k = g_k/\omega_k$, this unitary can be used to transform the spin-boson Hamiltonian (5.6), replacing the qubit-photon interaction with a renormalization of the

qubit levels

$$H_{LF} = U^\dagger H U = \frac{\hbar\Delta}{2}\sigma^z e^{-\sum 2\sigma^x (f_k a_k^\dagger - f_k^* a_k)} + \sum_k \hbar\omega_k a_k^\dagger a_k. \quad (5.27)$$

If we now adopt as a variational ansatz an arbitrary state for the qubit and coherent states for the bosons, $|\psi_{LF}\rangle = |\psi_{qb}\rangle \otimes_k |\alpha_k\rangle$, the result is that the minimal energy is achieved when all oscillator modes are in the vacuum, $\alpha_k = 0$, and the qubit is the ground state $|e\rangle$, of a renormalized Hamiltonian

$$H_{qb} = \frac{\hbar\tilde{\Delta}}{2}\sigma^z, \quad (5.28)$$

$$\tilde{\Delta} = \Delta e^{-\sum_k 4|g_k|^2/\omega_k^2} \leq \Delta. \quad (5.29)$$

Even if the ansatz predicts that ψ_{LF} is in the qubit ground state, the observables in the laboratory do not correspond to those of a depolarized qubit, because the actual observables have to be computed using the inverse unitary transformation

$$\langle\sigma_z\rangle = \langle\psi_{LF}| U^\dagger \sigma_z U |\psi_{LF}\rangle = e^{-\sum_k 4|g_k|^2/\omega_k^2} \leq \Delta. \quad (5.30)$$

In other words, the entanglement between the qubit and the photons introduced by U gives rise to a probability of the qubit being excited, and as $g \to \infty$, there is a phase transition to a state where the qubit in the lab is described by a classical mixture, $\rho = \frac{1}{2}(|g\rangle\langle g| + |e\rangle\langle e|)$.

The previous calculations are only qualitatively correct. They can be improved by leaving the complex numbers $\{f_k\}$ also as variational parameters. In this case they match very well the result from sophisticated numerical calculations based on Matrix-Product States or Density Matrix Renormalization Group [PZPGR13] —two numerical methods that can represent complex many-body wavefunctions of large one-dimensional problems. In figure 5.3 we show the result of a calculation with 128 modes using all these three models. Note how for very weak coupling, of less than 10% the qubit energy, the contributions to the polarization are negligible and grow as g^2. In this limit these corrections obtained by considering the counterrotating terms as off-resonant contributions that lead to virtual excitations of the qubit and the photons, and treating them with second order perturbation theory.

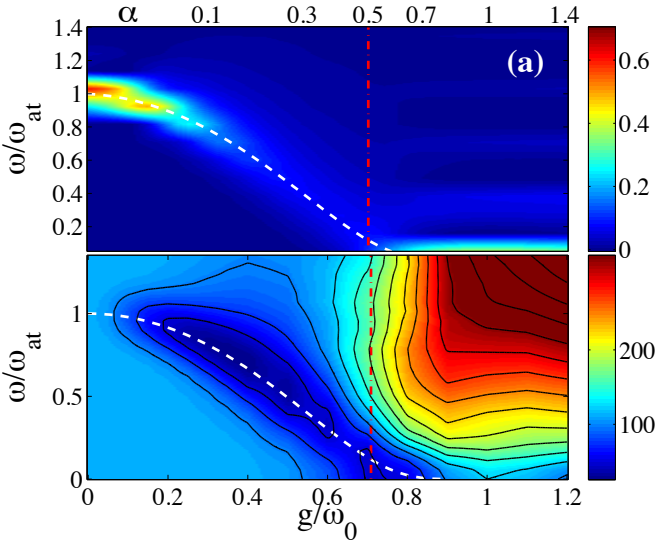

Figure 5.4: (a) Density of photons emitted into the transmission line by a superconducting qubit that relaxes to the ground state. We plot the density $n(\omega)$ as a function of the photon coupling and the intensity of the qubit-line coupling, measured either by α [cf. §5.1.3] or the ratio g/ω in a discretization with 128 bosonic modes [PZPGR13]. (b) Transmission rate for a single photon that impacts onto the same qubit. Note that (b) and (a) are related because spontaneous emission and scattering are converse proceses.

5.3.2 Spontaneous emission & scattering

When studying the dynamics of photons in stronger regimes of qubit-photon coupling we no longer have theoretical tools other than numerics. In figure 5.4 we show two different types of numerical experiments for a qubit that interact with the transmission line, as a function of the interaction strength parameter α [cf. §5.1.3].

The first plot, figure 5.4a, shows the number of photons in each mode of a discretized transmission line. This density of energy is computed simulating the time evolution of a qubit that is initially excited and in contact with a transmission line that contains no photons. After a long time, the whole system relaxes to a more or less equilibrium

state that contains one propagating photon and a qubit that is close to its ground state (not necessarily deexcited!). Once this has happened, we compute all observables $\langle a_k^\dagger a_k \rangle$ and obtain the typical frequency of the emitted photons.

Note how the frequency of the emitted photon is, for weak couplings, close to the original frequency of the qubit, Δ. As the coupling strength increases, the qubit frequency is renormalized with a formula that approximates (5.29), until it reaches zero at sufficiently large coupling strengths. At this point the qubit is "frozen", in the sense that it takes an exponentially large amount of time to induce any dynamics in it. In other words, the coupling terms $\sigma^x(a_k + a_k^\dagger)$ dominate the Hamiltonian and the qubit randomly collapses to one of the eigenstates of σ^x, with a negligible probability to transition to the other state.

Spontaneous emission is the converse process of scattering experiments. As illustrated in figure 5.1, an incoming photon that impacts on a qubit is partially absorbed and reemitted and it is the interference between these spontaneously emitted photon and the part of the photon that was not absorbed what determines the values of the transmission and reflection coefficients.

This fact is particularly obvious in figure **??**b, where we plot the transmission coefficient as a function of the coupling strength and the photon frequency. Around the same line on which the spontaneous emission frequency peaks, the transmission $T(\omega) \simeq 0$ becomes zero, indicating the fact that the qubit becomes a perfect mirror.

So, summing up, when we move beyond the RWA regime, several things happen: (i) the qubit always acts as a perfect mirror for a range of frequencies; (ii) the frequency of that resonance shifts down due to the dressing of the two-level system with a cloud of virtual photons; (iii) in addition to shifting, the resonance broadens, with a linewidth that can be as large as $25\%\Delta$; (iv) when the coupling is too strong, all dynamics ceases and the qubit becomes frozen.

Chapter 6

Circuit QED

As in AMO (Atomic and Molecular Optics), in superconducting circuits the most natural setup consists on a qubit that interacts with a variety of propagating electromagnetic modes, in the form of probes and control antennaes, but also the three-dimensional environment that surrounds the chip. However, for historic reasons, the explosion of superconducting quantum technologies and, to some extent, the birth of the field as we know it, starts not only with the design of the first qubits [1], but with a seminal experiment that studies a combined system of a qubit embedded in a microwave cavity [WSB+04]. The use of the cavity not only improved the lifetime of the qubit, due to the Purcell effect, but opened the door to a new experimental area, circuit-QED, in which microwave cavities and artificial atoms achieve what had been tried before with real atoms and optical cavities, cavity-QED.

In this chapter we review the setups and ideas behind circuit-QED, together with the main achievements and techniques that have made it possible not only some of the first quantum algorithms and computations in the field, but also to take Quantum Optics beyond what could be achieved with real matter so far. Similar to earlier chapters, we focus mostly on the RWA limit, which is the one that has been most thoroughly used in experiments, but provide a section on the so called ultrastrong coupling.

[1] See [?] for an overview of the field around 2001, shortly before the first circuit-QED experiments

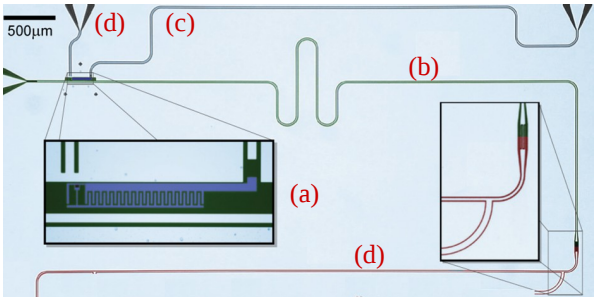

Figure 6.1: Fotograph of a transmon qubit standing near a microwave resonator. The picture shows a zoom of the qubit (a), the transmission line that forms the cavity (b, green), the line controlling the transmon gap (d) and the a line that interacts with the transmon to measure its state (c). Picture courtesy of A. Wallraff, with minor editions.

6.1 The Rabi model

6.1.1 Cavity-qubit interaction

Figure 6.1 summarizes many of the circuital elements that are part of a cavity-QED experiments with superconductors. The two obvious elements are the qubit (a) and the resonator (b). While there are many choices for the latter, most experiments settle with coplanar waveguide resonators and embed the qubit in the gap between the transmission line and the ground plane. The cavity is relatively simple and we only remark the capacitive coupling to a line (d, in red) which can be used to feed energy or read out the photons that leak from the cavity [cf. §3.5]

In this particular experiment the qubit is a transmon and there are two additional lines that control the qubit gap (d) and the qubit applied voltage (c). Note how the transmon qubit is built with a SQUID loop in place of the junction. The line (d) circulates some current that sinks into the ground plane but is strong enough to induce a magnetic field that, after circulating through the SQUID, induces significant changes in the transmon inductance and its gap at zero bias. The line (c), on the other hand, can be used to induce additional voltages (note how it is capacitively coupled to one layer of the capacitor) and also for

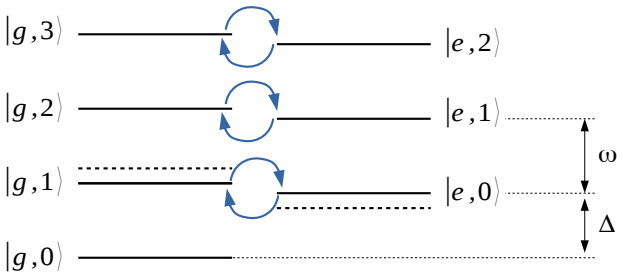

Figure 6.2: Energy level structure of a qubit and a cavity without coupling (solid), as described by the Jaynes-Cummings model (6.2). When the interaction is switched on, states $|g, n\rangle$ and $|e, n-1\rangle$ get coupled, leading to new eigenstates that are superpositions (dashed) and which are shifted from their original energies.

readout.

The effective Hamiltonian that models the qubit-cavity interaction is the so called Rabi model

$$H = \hbar\omega a^\dagger a + \hbar g \sigma^x (a + a^\dagger) + \frac{\hbar\Delta}{2}\sigma^z, \tag{6.1}$$

which is nothing but an extreme case of the spin-boson model (5.6), in a situation in which the spectrum of photons is gapped and there is only one mode that is close to resonance with the qubit.

As in the case of the open transmission line, however, the coupling strength g is the smallest time scale in that problem and we can apply the rotating wave approximation, obtaining the Jaynes-Cummings model

$$H = \hbar\omega a^\dagger a + \hbar g (\sigma^+ a + a^\dagger \sigma^-) + \frac{\hbar\Delta}{2}\sigma^z. \tag{6.2}$$

This is a much simpler Hamiltonian which, as in its free space relative, conserves the total number of excitations. Photons are therefore oscillating back and forth between the qubit and the cavity, and the Hamiltonian becomes box diagonal.

6.1.2 Vacuum Rabi splitting

The Jaynes-Cummings model gives rise to an interesting dynamics between the cavity and the qubit, which is summarized in figure 6.2. The total number of excitations

$$N_e = |e\rangle\langle e| + a^\dagger a, \tag{6.3}$$

is thereby conserved. The coupling term $\sigma^+ a + \sigma^- a$ is box diagonal and only relates the state $|g, n+1\rangle$ with its neighbor $|e, n\rangle$, through a process in which the qubit absorbs a photon from the cavity and gets excited.

Mathematically, within the subspace $\{|g, n+1\rangle, |e, n\rangle\}$, the Hamiltonian acquires a box-diagonal structure

$$H_n = \hbar\omega(n + \tfrac{1}{2}) + \frac{\hbar(\Delta - \omega)}{2}\sigma^z + \frac{\hbar g\sqrt{n+1}}{2}\sigma^x. \tag{6.4}$$

This Hamiltonian block has two eigenstates with eigenenergies

$$E_{n,\pm} = \hbar\omega(n + \tfrac{1}{2}) \pm \frac{1}{2}\sqrt{(\Delta - \omega)^2 + g^2(n+1)}. \tag{6.5}$$

In particular, in the resonant case, the two lowest energy excitations right about the ground state $|g, 0\rangle$ have energies $E_{0,\pm} = \hbar(\omega \pm g)/2$. Therefore, transitions from the actual ground state, $E_{gs} = -\hbar$ $omega/2$, to either of these states will have frequencies $\omega \pm g/2$, with two resonances that spread a part a distance g.

These transitions can be probed experimentally through an spectroscopy experiment. Injecting microwave photons through one side of the cavity, and looking at the other side, we should see transmitted photons only when they are resonant with one of the allowed transitions. In figure 6.3a we show the transmission spectra for $\Delta = \omega$. Notice how the two maxima of transmission spread apart linearly as a function of g.

Alternatively we can change the qubit frequency in and out of resonance with the cavity, leaving the coupling fixed. This is shown in figure 6.3b. In this numerical experiment we fix $g = 0.05\omega$ and the qubit gap $\Delta = 0.7\omega$, and apply an external field ϵ, that changes the qubit energy splitting. When the qubit is strongly off-resonant from the cavity, transmission can only happen by injecting one photon into

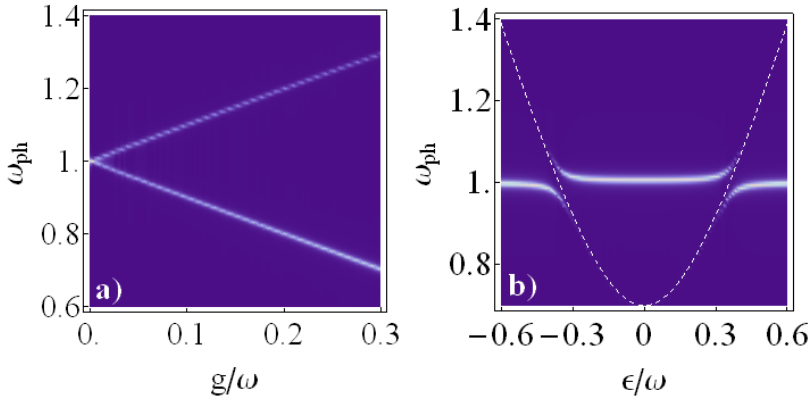

Figure 6.3: (a) Transmission through the cavity as a function of the relative coupling, for $\omega = \Delta$. (b) Transmission through the cavity as a function of the qubit bias, ε, for $\Delta = 0.7\omega$ and $g = 0.05\omega$. In dashed line we plot the qubit energy levels for $g = 0$. The linewidths assume $\sqrt{\gamma\kappa} = 0.005\omega$.

the system and allowing that photon to leak through either side of the cavity. The transitions that drive this process are $|s, n\rangle \rightarrow |s, n+1\rangle$, and the state of the qubit, $s \in \{g, e\}$, is unaltered. These transitions have a resonance at ω, which is the frequency at which the horizontal line of maxima happens. If we now apply the external field and bring the qubit frequency to resonance with the cavity (dashed line in figure 6.3b), $\sqrt{\Delta^2 + \epsilon^2} \simeq \omega$, it now becomes possible to have processes such as those from figure 6.2 and the original resonance splits into two, corresponding to the two allowed transitions. In the plot 6.3b this is seen in the form of an avoided crossing where the minimal separation between spectroscopy lines is g.

6.1.3 Weak, strong and ultrastrong coupling limits

Can the vacuum Rabi splitting be seen in an experiment? It depends mainly on the properties of the cavity. The linewidth of these resonances is proportional to the qubit and cavity decoherence rates, γ and κ. If these lines are broader than the splitting, $\sqrt{\kappa\gamma} > g$, the experiment is found in the *weak coupling* regime and the lines cannot be

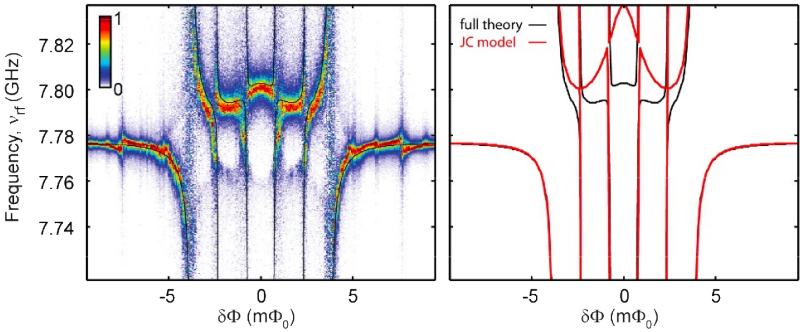

Figure 6.4: (left) Transmission spectroscopy results for a flux qubit interacting with the third mode of a microwave resonator. (right) Two different fits with the RWA and Jaynes-Cummings (red) and the full Rabi model (black).

resolved spectroscopically.

This was the situation in most experiments with atoms in a cavity until recently, and it is the situation of optomechanical devices nowadays, due to the difficulty of building high-quality cavities with large couplings to the optical transitions of the embedded system. However, as we have seen through these notes, microwave cavities have very little losses and they can be tuned by changing their capacitive and inductive interactions to nearby elements. Moreover, superconducting qubits and microwave cavities are made of the same material,1 and photons and charge/flux excitations may be regarded as two sides of the same coin. It is therefore natural that one can reach high ratios that allow the observation of the Rabi splitting.

This is indeed what was achieved in the seminal work by the Yale group in 2004 [WSB$^+$04]. In that experiment, a cavity with a frequency of around $\omega/2\pi \simeq 6GHz$ was designed to have a quality factor $Q = 10^4$, These losses, $\kappa = 2\pi \times 0.8$ MHz, were mainly due to leakage through the extremal capacitors at the ends of the line, the internal losses of the photon being two orders of magnitude smaller. Adjusting spectra similar to the ones in figure 6.3b, it was possible for them to fit the qubit parameters, the coupling $g/2\pi = 11$ MHz, and the qubit decoherence rate $\gamma/2\pi = 0.8$MHz.

Experiments in the last years have improved to the point that g need no longer be limited to 11MHz. Setups with flux qubits can be designed so that the qubit and the photons to share a piece of the transmission line, increasing the coupling strength to limits around $g \simeq \omega$ [**?**]. This idea has been experimentally tested in two different setups, one with a microwave transmission line resonator [**?**] with multiple modes and a different one with a flux qubit coupled to a zero mode LC resonator [**?**]. In figure 6.4 we show a transmission spectrum from experiment [**?**]. This particular spectrum is centered on the third resonator mode of the transmission line, with an enhanced coupling $g/\omega \simeq 12\%$ based on the previous ideas. As shown in figure 6.4b this spectrum is only fitted properly when we consider both the rotating and counterrotating terms, that is the full Rabi model (6.1). This regime of couplings is known as the *ultrastrong coupling regime*.

6.2 Circuit-QED control

6.2.1 Off-resonant limit

6.2.2 Qubit measurement and spectroscopy

6.2.3 State engineering

Appendix A

Appendices

A.1 Number-phase representation

Our quantisation procedure is based on the commutation relation $[\hat{\phi}, \hat{q}] = i\hbar$, that equates charge and flux to position and momentum. In practice, however, the charge q is not quite like the momentum operator, because it is defined in multiples of the charge quantum, $-2e$. Similarly, $\hat{\phi}$ is not at all like the position operator, but it is rather related to the phase of the superconductor wavefunction and thus periodic in units of the flux quantum Φ_0.

It is therefore possible to draw a relation between the flux-charge operators and a possible phase-number representation that would implement such operators. Unfortunately, defining a unique phase-number representation with the desired properties is a daunting task and we will only use some minor ideas that are sufficient for our computations, leaving subtleties behind. Our notation is consistent with [PB89] and with the original definition of the phase operator by Susskind and Glogower [SG64].

The eigenstates of the charge operator are the number states

$$\hat{q}\,|n\rangle = -2e \times n\,|n\rangle\,, \quad n \in \mathbb{Z}. \tag{A.1}$$

A possible representation of these states is given by the exponentials of the phase operator

$$\hat{\varphi} = \frac{\hat{\phi}}{\varphi_0} \tag{A.2}$$

giving eigenfunctions that are defined over the phase circle, periodically

$$|n\rangle \sim \frac{1}{\sqrt{2\pi}} e^{-in\varphi}, \quad \varphi \in [0, 2\pi). \tag{A.3}$$

In this representation the number operator is the generator of translations and is proportional to the charge

$$\hat{q} = -2e\hat{n} = -2e(i\partial_\varphi). \tag{A.4}$$

The phase operator, on the other hand, is proportional to the flux and is the generator of charge increments and decrements

$$e^{-im\varphi}\hat{n}e^{-im\varphi} = \hat{n} - m, \tag{A.5}$$

$$e^{-im\varphi}|n\rangle = |n+1\rangle, \tag{A.6}$$

or in the Susskind notation

$$e^{im\varphi} = \sum_{n\in\mathbb{Z}} |n\rangle\langle n+1|. \tag{A.7}$$

It is no surprise then, that we can write the Josephson energy as a tunnelling term

$$\cos(\varphi) = \frac{1}{2}\sum_n |n+1\rangle\langle n| + \text{H.c.} \tag{A.8}$$

that is responsible for the transport of charge across the junction.

An important subtlety of this problem is that phase and number, $\hat{\varphi}$ and $\hat{n}$, do not satisfy the same commutation relations as flux and charge. Because of the periodic boundary conditions, we have

$$[\hat{\varphi}, \hat{n}] = -i\sum_{m\in\mathbb{Z}} \delta(\varphi - 2\pi m). \tag{A.9}$$

and only when the wavefunction is localized in the phase space, do these commutators approach the position-momentum one.

A.2 Josephson junctions and the Mathieu equation

The Hamiltonian for a Josephson junction, a charge qubit or a transmon read always

$$H = \frac{1}{2C}q^2 - E_J\cos(\phi/\varphi_0). \tag{A.10}$$

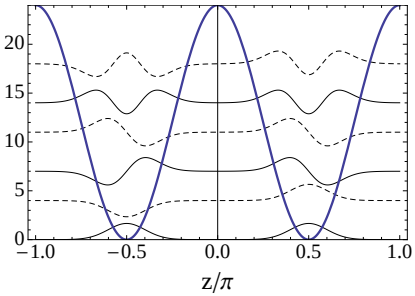

Figure A.1: The eigenfunctions generated by `MathieuC` (solid) and `MathieuS` (dash) for positive $q = 25$. Functions have been arbitrarily shifted to aid readability. Note that the potential that traps them, $2q\cos(2z)$, has the minima at $z = \pm\pi/2$ because $q > 0$.

Following §A.1, we can use the phase representation to write the associated Schrödinger equation as follows

$$\left[4E_C(-i\partial_\varphi)^2 - E_J\cos(\varphi)\right]\psi_n(\varphi) = \varepsilon_n\psi_n(\varphi). \tag{A.11}$$

This equation has to be compared to the Mathieu differential equation, which following Mathematica's notation reads

$$\frac{d^2}{dz^2}u(z) + [a - 2q\cos(2z)]u(z) = 0. \tag{A.12}$$

This equation has as solution two special functions, denoted $C(a, q, z)$ and $S(a, q, z)$ to represent generalized cosine (even) and sine (odd) functions. We are only interested in the solutions C and S which have the appropriate 2π periodicity of the phase. This periodicity only happens for values of the parameter a that we identify with the eigenenergies of the problem. More precisely

- `MathieuC[a,q,z]` and `MathieuS[a,q,z]` return even and odd eigenfunctions for parameters a and q.
- `MathieuCharacteristicA[r,q]` and `MathieuCharacteristicB[r,q]` return the eigenenergies, sorted by integer number r.

In practice Mathematica does not work well with negative values of q, which are the ones we need ($q = -E_J/2E_C$ in our model). However,

it is not hard to realize that changing $q \to -q$ amounts to a shift $z \to z \pm \pi/2$ (cf. figure A.1), so that (i) all eigenenergies are the values of `MathieuCharacteristicA[r,EJ/(2*EC)]` for integer $r = 0, 1, \ldots$ and (ii) all eigenfunctions are `MathieuC[E,EJ/(2*EC),z]`, where $z = (\varphi - \pi)/2$.

A.3 Tridiagonal matrix diagonalization

Periodic boundary conditions

We need to diagonalize the matrix

$$B = \begin{pmatrix} a & b & 0 & \ldots & 0 & 0 & b \\ b & a & b & \ldots & 0 & 0 & 0 \\ 0 & b & a & \ldots & 0 & 0 & 0 \\ \vdots & \vdots & \vdots & \ddots & \vdots & & \\ 0 & 0 & 0 & \ldots & a & b & 0 \\ 0 & 0 & 0 & \ldots & b & a & b \\ b & 0 & 0 & \ldots & 0 & b & a \end{pmatrix} \in \mathbb{R}^{N \times N}. \tag{A.13}$$

The eigenmodes are defined by the eigenvalue equations

$$b(u_{m-1} + u_{m+1}) + a u_m = \lambda u_m, \quad m = 1 \ldots N \tag{A.14}$$

where we need the identification $u_{m+N} = u_m$ associated to periodic boundary conditions.

We can solve the eigenvalue equations with plane waves

$$u_m^{(n)} = \frac{1}{\sqrt{N}} \exp(i k_n m), \quad k_n = \frac{2\pi n}{N} \in \frac{2\pi}{N} \times \{0, 1, 2 \ldots N-1\}, \tag{A.15}$$

that naturally satisfy the boundary conditions, $u_{m+N} = u_m \exp(ikN) = u_m \exp(i2\pi n)$. The eigenvalues associated form a band

$$\lambda_n = a + 2b \cos(k_n). \tag{A.16}$$

Note that the actual momenta, k_n, can take any value up to displacements of order 2π. It is quite often more convenient to choose these

labels so that they explore the interval $(-\pi, \pi]$, instead of $[0, 2\pi)$, as defined above. In this case we choose

$$k_n \in \frac{\pi}{2M} \times \{-M+1, -M+2, \ldots -1, 0, 1 \ldots M\}, \tag{A.17}$$

for even sizes $N = 2M$ and

$$k_n \in \frac{\pi}{2M+1} \times \{-M, -M+1, \ldots -1, 0, 1 \ldots M\}, \tag{A.18}$$

for odd ones, $N = 2M + 1$.

It is also sometimes interesting to replace the complex wavefunctions $e^{ik_n m}$ with real ones. In other words, instead of diagonalizing B with a unitary transformation, we use an orthogonal one, $B = O^T \Lambda O$, $O \in \mathbb{R}^{N \times N}$, $O^T O = 1$. The eigenfunctions are linear combinations of the exponentials, consisting on sinusoidal functions

$$\begin{aligned} u_m^{(even,n)} &= \sqrt{\frac{2}{N}} \cos(k_n m), \quad k_n \in (0, \pi) \\ u_m^{(odd,n)} &= \sqrt{\frac{2}{N}} \sin(k_n m), \end{aligned} \tag{A.19}$$

plus the two extra solutions

$$u_m^{(even,0)} = \sqrt{\frac{1}{N}}, \quad k_0 = 0, \tag{A.20}$$

$$u_m^{(even,n)} = \sqrt{\frac{1}{N}} (-1)^m, \quad k_n = \pi. \tag{A.21}$$

Open boundary conditions

We need to diagonalize the matrix

$$B = \begin{pmatrix} a & b & 0 & \ldots & 0 & 0 & 0 \\ b & a & b & \ldots & 0 & 0 & 0 \\ 0 & b & a & \ldots & 0 & 0 & 0 \\ \vdots & \vdots & \vdots & \ddots & \vdots & & \\ 0 & 0 & 0 & \ldots & a & b & 0 \\ 0 & 0 & 0 & \ldots & b & a & b \\ 0 & 0 & 0 & \ldots & 0 & b & a \end{pmatrix} \in \mathbb{R}^{N \times N}. \tag{A.22}$$

The eigenmodes are defined by the eigenvalue equations

$$\begin{aligned} b(u_{m-1}+u_{m+1})+bu_m &= \lambda u_m, \quad m=2\dots N-1 \\ bu_2+au_1 &= \lambda u_1, \\ bu_{N-1}+au_N &= \lambda u_N. \end{aligned} \tag{A.23}$$

A trick to solve this problem is to realize that these equations are equivalent to those of a periodic boundary condition problem (A.14) of size $2(N+1)$, where one imposes $u_{N+1} = u_{2(N+1)} = 0$. Such as solution may be constructed by combining two plane waves that have opposite momenta and are thus degenerate eigenmodes of the periodic boundary conditions problem

$$u_m \propto e^{ikm} - e^{-ikm} \tag{A.24}$$

We summarize here the final solution, including the appropriate normalization factors

$$u_m = \sqrt{\frac{2}{N}}\sin(k_n m), \tag{A.25}$$

$$\begin{aligned} k_n &\in \frac{\pi}{N+1}\times\{1,2,\dots N\} \\ \lambda_n &= a+2b\cos(k_n). \end{aligned} \tag{A.26}$$

Note that, unlike in the periodic case, we can no longer shift the linear momenta, which are constrained to the interval $[0,\pi)$.

A.4 Harmonic chain diagonalization

We are going to diagonalize a problem of coupled Harmonic oscillators, which we write in the following form:

$$H = \frac{1}{2C}\mathbf{p}^T\mathbf{p} + \frac{1}{2L}\mathbf{x}^T B\mathbf{x}. \tag{A.27}$$

We will use that the position and momentum operators can be defined in terms of N Fock operators, with commutation relations $[b_n, b_m^\dagger] = \delta_{nm}$. The relation between both operators is given by

$$x_m = \sum_n a_n \frac{1}{\sqrt{2}}(U_{mn}b_n + U_{mn}^* b_n^\dagger), \tag{A.28}$$

$$p_m = \sum_n \frac{\hbar}{a_n}\frac{i}{\sqrt{2}}(U_{mn}^* b_n^\dagger - U_{mn}b_n), \tag{A.29}$$

where a_n are non-negative constants and U is a unitary transformation. Using $U^*_{nm}U_{nr} = \delta_{mr}$, we can prove that the commutation relations between position and momenta are satisfied, $[x_m, x_r] = 0$, $[p_m, p_r] = 0$, $[x_m, p_r] = i\hbar\delta_{mr}$.

How do we use this? Let us assume that matrix $B \in \mathbb{R}^{N\times N}$, which is real and symmetric, is diagonalized with an orthogonal transformation

$$B = U^\dagger \Lambda U, \text{ with } \begin{cases} \Lambda_{ij} = \lambda_i \delta_{ij} \\ U^T U = 1,\ U \in \mathbb{R} \end{cases} \tag{A.30}$$

Thanks to the orthogonality condition we can write

$$\mathbf{p}^T\mathbf{p} = \sum_m \frac{\hbar^2}{2a_n^2}(b_n^\dagger b_n + b_n b_n^\dagger - b_n^{\dagger\,2} - b_n^2) \tag{A.31}$$

$$\mathbf{x}^T B\mathbf{x} = \sum_m \frac{a_n^2\lambda_n}{2}(b_n^\dagger b_n + b_n b_n^\dagger + b_n^{\dagger\,2} + b_n^2) \tag{A.32}$$

We impose the conditions

$$\frac{\hbar^2}{2Ca_n^2} = \frac{a_n^2\lambda}{2L} = \frac{1}{2}\hbar\omega_n. \tag{A.33}$$

This gives the frequencies and oscillator lengths

$$\omega_n = \sqrt{\frac{\lambda_n}{CL}},\ a_n = \sqrt{\frac{\hbar}{C\omega_n}}, \tag{A.34}$$

and the Hamiltonian becomes diagonal

$$H = \sum_n \hbar\omega_n \left(b_n^\dagger b_n + \frac{1}{2}\right). \tag{A.35}$$

Periodic boundary conditions

In a problem with periodic boundary conditions, with $B_{ij} = B_{i+1j+1}$, the matrix B can be diagonalized with two sets of wavefunctions, either sines and cosines or complex exponentials [cf. §A.3]. The time reversal associated to real couplings B causes pairs of momenta $\pm k$ to be degenerate in frequency, so that wavefunctions $\cos(kx)$ and $\sin(kx)$ or

any combination of them can be used. If we call b_{ck} and b_{sk} the Fock operators, we introduce

$$b_{\pm k} = \frac{1}{\sqrt{2}}(b_{ck} \pm i b_{sk}),\ k \neq 0, \pi \tag{A.36}$$

$$b_{0,\pi} = b_{c0,\pi}. \tag{A.37}$$

According to this definition

$$x_m = \sum_k a_n \frac{1}{\sqrt{2N}} \left(e^{ikm} b_k + e^{-ikm} b_k^\dagger \right), \tag{A.38}$$

$$p_m = \sum_k \frac{\hbar}{a_n} \frac{i}{\sqrt{2N}} (e^{-ikm} b_n^\dagger - e^{ikm} b_n), \tag{A.39}$$

where the sum takes place over the allowed values of the quasimomentum k, including the special cases $k = 0$ and π, where originally and also here there is only one mode. The diagonalized Hamiltonian takes the expected form

$$H = \sum_k \omega_k b_k^\dagger b_k, \tag{A.40}$$

with the degeneracy $\omega_k = \omega_{-k}$.

A.5 Master equations

A.5.1 Interaction picture

Let us assume that the Hamiltonian of our system can be separated into two parts, $H = H_0 + H_1$. Typically, H_1 will be a perturbation of a problem H_0 that we can solve exactly. The evolution of the full system is generated by a unitary operator $U(t)$ that satisfies the Schrödinger equation,

$$i\frac{d}{dt}U(t) = (H_0 + H_1)U(t), \tag{A.41}$$

with initial condition $U(0) = 1$.

We split the evolution operator into two contributions, $U(t) = \exp(-iH_0 t)W(t)$. The first part, as we mentioned before, can be solved exactly, while the second contribution, W, groups the new dynamics produced by the perturbation H_1

$$i\frac{d}{dt}W(t) = e^{iH_0 t} H_1 e^{-iH_0 t} W(t) = H_1(t)W(t). \tag{A.42}$$

In what follows we will use this equation recursively, profiting from the fact that $H_1(t)$ is a small correction and we can consider its contributions perturbatively.

A.5.2 Lindblad equation

We start with a problem in the interaction picture, described by a time-dependent Hamiltonian, $H_1(t)$, that describes the coupling between a small system and larger environment or bath. The state of the combined system will be described by a density matrix $\rho(t)$, evolving with the master equation

$$\frac{d}{dt}\rho(t) = -\frac{i}{\hbar}[H_1(t), \rho(t)]. \tag{A.43}$$

Because H_1 is a small perturbation, we feel confident to use perturbation theory up to second order. Thus, starting from a state $\rho(t)$, after a time δt will be given by the Dyson formula

$$\begin{aligned} \rho(t+\delta t) &\simeq \rho(t) - \frac{i}{\hbar}\int_t^{t+\delta t} [H_1(t'), \rho(t)]\mathrm{d}t' \\ &- \frac{1}{\hbar^2}\int_t^{t+\delta t}\int_t^{t'} [H_1(t'), [H_1(t''), \rho(t)]]\mathrm{d}t''\mathrm{d}t'. \end{aligned} \tag{A.44}$$

At this point we make our second approximation, which is to assume that the feedback of the system onto the environment is negligible. Because the environment is so large, we can assume that it remains approximately in the same state, so that $\rho(t) = \rho_S(t) \otimes \rho_B$. We can thus focus on the evolution of the system, tracing out all other degrees of freedom and in doing so we will impose[1] $\mathrm{Tr}_B\{H_1(t')\rho(t)\} = 0$. We thus obtain

$$\rho_S(t+\delta t) \simeq \rho_S(t) - \frac{1}{\hbar^2}\int_t^{t+\delta t}\int_t^{t'} \mathrm{Tr}_B[H_1(t'), [H_1(t''), \rho_S(t)\otimes\rho_B]]\mathrm{d}t''\mathrm{d}t'.$$

In what follows, we will show how this equation may be approximated as a linear transformation of the density matrix,

$$\rho_S(t+\delta t) = \rho_S(t) + \delta t\mathcal{L}\rho_S(t), \tag{A.45}$$

[1] We will see that this is not really a restriction, as typically $H_1 \sim O_S \otimes O_B$, where the system and bath operators O_S and O_B have zero diagonal elements

so that we may write the Lindblad equation

$$\frac{d}{dt}\rho_S = \mathcal{L}\rho_S \tag{A.46}$$

Note that in this equation the superoperator[2] $\mathcal{L}$ is time independent. In other words, the evolution of the system only at time t only depends on that instant of time and not on the earlier history. This property is called Markovianity and arises from a certain behavior of the interaction Hamiltonian and the spectrum of the unperturbed model, H_0.

A.5.3 Linear system-bath coupling

In many of the problems that we find throughout these notes, the system bath interaction may be written

$$H_1 = A^\dagger \sum_k B_k + \text{H.c.}, \tag{A.47}$$

with some system operator A and some bath operators B_k. In the interaction picture the frequency of the system will be Δ, while that of the bath will change from mode to mode, ω_k:

$$H_1(t) = A^\dagger e^{i\Delta t} \sum_k g_k B_k e^{-i\omega_k t} + \text{H.c.} = \tag{A.48}$$

When we insert this expression into the formula (A.45), we obtain four terms that arise from the different combinations of A and B operators multiplying ρ

$$\Delta\rho_S = \int_t^{t+\delta t} \mathrm{d}t \left\{ I_{B^\dagger B^\dagger}\mathcal{L}_{AA} + I_{B^\dagger B}\mathcal{L}_{AA^\dagger} + I_{BB^\dagger}\mathcal{L}_{A^\dagger A} + I_{BB}\mathcal{L}_{A^\dagger A^\dagger} \right\} \rho_S(t). \tag{A.49}$$

The Lindblad operators in this expression have all similar forms

$$\mathcal{L}_{XY}\rho = 2X\rho Y - YX\rho - \rho YX, \tag{A.50}$$

[2] A superoperator is a linear transformation that maps operators into other operators in the same space.

and the integrals are

$$
\begin{aligned}
I_{BB} &= \sum_{pq} g_p g_p \int_t^{t+\delta t} \langle B_p B_q \rangle \, e^{-i(\omega_p-\Delta)t - i(\omega_q-\Delta)t'} \quad \text{(A.51)} \\
I_{BB^\dagger} &= \sum_{pq} g_p g_p^* \int_t^{t+\delta t} \langle B_p B_q^\dagger \rangle \, e^{-i(\omega_p-\Delta)t + i(\omega_q-\Delta)t'} \\
I_{B^\dagger B} &= \sum_{pq} g_p^* g_p \int_t^{t+\delta t} \langle B_p^\dagger B_q \rangle \, e^{+i(\omega_p-\Delta)t - i(\omega_q-\Delta)t'} \\
I_{B^\dagger B^\dagger} &= \sum_{pq} g_p^* g_p^* \int_t^{t+\delta t} \langle B_p^\dagger B_q^\dagger \rangle \, e^{+i(\omega_p-\Delta)t + i(\omega_q-\Delta)t'}.
\end{aligned}
$$

We will argue that each of these integrals is approximately independent of time and thus confirms our original idea of producing a Markovian master equation.

If we focus on thermal baths, only the $I_{BB^\dagger}$ and $I_{B^\dagger B}$ terms survive, because

$$
\begin{aligned}
\langle B_q B_p \rangle &= \langle B_q^\dagger B_p^\dagger \rangle = 0, \quad \text{(A.52)} \\
\langle B_q^\dagger B_p \rangle &= n(\omega_p)\delta_{q,p}, \quad \text{(A.53)} \\
\langle B_q B_p^\dagger \rangle &= (n(\omega_p)+1)\delta_{q,p}. \quad \text{(A.54)}
\end{aligned}
$$

We can now introduce the spectral function

$$
J(\omega) = 4\pi \sum_k |g_k|^2 \delta(\omega - \omega_k), \quad \text{(A.55)}
$$

by which

$$
I_{B^\dagger B} = \int_t^{t+\delta t} \mathrm{d}t \int \frac{\mathrm{d}\omega}{4\pi} J(\omega) n(\omega) e^{i(\omega-\Delta)(t-t')}. \quad \text{(A.56)}
$$

The Markovian assumption enters by assuming that J and n are smooth functions and the integral itself decays very rapidly with time, in a memory time $\tau \ll \delta t$. Following [WM94], this allows us to take the upper integration limits to $\pm\infty$, recovering the distribution

$$
\int_0^\infty \mathrm{d}\tau e^{i\epsilon\tau} = \pi\delta(\epsilon) - iPV\left(\frac{1}{\epsilon}\right), \quad \text{(A.57)}
$$

where $\tau = t - t'$ and $\epsilon = \omega - \Delta$. When we push this distribution into the formula for $I_{B^\dagger B}$ we find

$$I_{B^\dagger B} = \frac{\gamma}{2} n(\omega) + i\tilde{\Delta}, \tag{A.58}$$

with the small correction to the system frequency called the Lamb shift

$$\tilde{\Delta} = \mathrm{PV} \int_{-\infty}^{\infty} \frac{\mathrm{d}\epsilon}{4\pi} \frac{1}{\epsilon} J(\Delta + \epsilon) n(\Delta + \epsilon) \simeq 0, \tag{A.59}$$

and a heating rate $\gamma = J(\Delta)/2$. A similar computation gives

$$I_{BB^\dagger} = \frac{\gamma}{2}[n(\Delta) + 1] + i\tilde{\Delta}'. \tag{A.60}$$

When we inject these formulas into equation (A.49), we obtain the usual Quantum Optics textbook material

$$\begin{aligned} \frac{d}{dt}\rho_S &= [n(\Delta) + 1]\frac{\gamma}{2}\left(2A\rho A^\dagger - A^\dagger A\rho - \rho A^\dagger A\right) \\ &+ n(\Delta)\frac{\gamma}{2}\left(2A^\dagger \rho A - AA^\dagger \rho - \rho AA^\dagger\right), \end{aligned} \tag{A.61}$$

with the cooling and heating Lindblad operators.

Bibliography

[BLP+07] Douglas A Bennett, Luigi Longobardi, Vijay Patel, Wei Chen, and James E Lukens. rf-SQUID qubit readout using a fast flux pulse. *Superconductor Science and Technology*, 20(11):S445–S449, November 2007.

[CB04] John Clarke and Alex I. Braginski, editors. *The SQUID Handbook: Fundamentals and Technology of SQUIDs and SQUID Systems, Volume I.* Wiley-VCH, Weinheim, 2004.

[CW08] John Clarke and Frank K Wilhelm. Superconducting quantum bits. *Nature*, 453(7198):1031–42, June 2008.

[Dev95] MH Devoret. Quantum fluctuations in electrical circuits. *Les Houches, Session LXIII*, pages 351–386, 1995.

[DiV95] D. P. DiVincenzo. Quantum Computation. *Science*, 270(5234):255–261, October 1995.

[HBJ+07] R. Harris, A. Berkley, M. Johnson, P. Bunyk, S. Govorkov, M. Thom, S. Uchaikin, A. Wilson, J. Chung, E. Holtham, J. Biamonte, A. Smirnov, M. Amin, and Alec Maassen van den Brink. Sign- and Magnitude-Tunable Coupler for Superconducting Flux Qubits. *Physical Review Letters*, 98(17):177001, April 2007.

[HKP+13] Io-Chun Hoi, Anton F. Kockum, Tauno Palomaki, Thomas M. Stace, Bixuan Fan, Lars Tornberg,

Sankar R. Sathyamoorthy, Göran Johansson, Per Delsing, and C. M. Wilson. Giant Cross–Kerr Effect for Propagating Microwaves Induced by an Artificial Atom. *Physical Review Letters*, 111(5):053601, August 2013.

[HWA+09] Max Hofheinz, H Wang, M Ansmann, Radoslaw C Bialczak, Erik Lucero, M Neeley, A D O'Connell, D Sank, J Wenner, John M Martinis, and A N Cleland. Synthesizing arbitrary quantum states in a superconducting resonator. *Nature*, 459(7246):546–9, May 2009.

[KYG+07] Jens Koch, Terri Yu, Jay Gambetta, A. Houck, D. Schuster, J. Majer, Alexandre Blais, M. Devoret, S. Girvin, and R. Schoelkopf. Charge-insensitive qubit design derived from the Cooper pair box. *Physical Review A*, 76(4), October 2007.

[LCD+87] A. Leggett, S. Chakravarty, A. Dorsey, Matthew Fisher, Anupam Garg, and W. Zwerger. Dynamics of the dissipative two-state system. *Reviews of Modern Physics*, 59(1):1–85, January 1987.

[LKOH+05] Julien Laurat, Gaëlle Keller, José Augusto Oliveira-Huguenin, Claude Fabre, Thomas Coudreau, Alessio Serafini, Gerardo Adesso, and Fabrizio Illuminati. Entanglement of two-mode Gaussian states: characterization and experimental production and manipulation. *Journal of Optics B: Quantum and Semiclassical Optics*, 7(12):S577–S587, December 2005.

[MOL+99] J. E. Mooij, T. P. Orlando, L. Levitov, L. Tian, C. H. van der Wal, and S. Lloyd. Josephson Persistent-Current Qubit. *Science*, 285(5430):1036–1039, August 1999.

[PB89] D. Pegg and S. Barnett. Phase properties of the quantized single-mode electromagnetic field. *Physical Review A*, 39(4):1665–1675, February 1989.

[PZPGR13] B. Peropadre, D. Zueco, D. Porras, and J. García-Ripoll. Nonequilibrium and Nonperturbative Dynamics of Ultrastrong Coupling in Open Lines. *Physical Review Letters*, 111(24):243602, December 2013.

[RGRS09] Guillermo Romero, Juan José García-Ripoll, and Enrique Solano. Photodetection of propagating quantum microwaves in circuit QED. *Physica Scripta*, T137(T137):014004, December 2009.

[SF05a] J. T. Shen and Shanhui Fan. Coherent photon transport from spontaneous emission in one-dimensional waveguides. *Optics Letters*, 30(15):2001, 2005.

[SF05b] Jung-Tsung Shen and Shanhui Fan. Coherent Single Photon Transport in a One-Dimensional Waveguide Coupled with Superconducting Quantum Bits. *Physical Review Letters*, 95(21):213001, November 2005.

[SG64] L. Susskind and J. Glogower. Quantum mechanical phase and time operator. *Physics*, 1:49–61, 1964.

[SHK+08] J. Schreier, A. Houck, Jens Koch, D. Schuster, B. Johnson, J. Chow, J. Gambetta, J. Majer, L. Frunzio, M. Devoret, S. Girvin, and R. Schoelkopf. Suppressing charge noise decoherence in superconducting charge qubits. *Physical Review B*, 77(18), May 2008.

[SWP+08] M. Sandberg, C. M. Wilson, F. Persson, T. Bauch, G. Johansson, V. Shumeiko, T. Duty, and P. Delsing. Tuning the field in a microwave resonator faster than the photon lifetime. *Applied Physics Letters*, 92(20):203501, May 2008.

[SZ67] A. Silver and J. Zimmerman. Quantum States and Transitions in Weakly Connected Superconducting Rings. *Physical Review*, 157(2):317–341, May 1967.

[vdWtHW+00] C. H. van der Wal, A C ter Haar, F K Wilhelm, R N Schouten, C J Harmans, T P Orlando, S Lloyd, and J E Mooij. Quantum Superposition of Macroscopic

Persistent-Current States. *Science*, 290(5492):773–777, October 2000.

[WJP+11] C M Wilson, G Johansson, A Pourkabirian, M Simoen, J R Johansson, T Duty, F Nori, and P Delsing. Observation of the dynamical Casimir effect in a superconducting circuit. *Nature*, 479(7373):376–9, November 2011.

[WM94] D. F. Walls and G. J. Milburn. *Quantum Optics*. Springer Berlin Heidelberg, Berlin, Heidelberg, 1994.

[WPGP+12] Christian Weedbrook, Stefano Pirandola, Raúl García-Patrón, Nicolas J. Cerf, Timothy C. Ralph, Jeffrey H. Shapiro, and Seth Lloyd. Gaussian quantum information. *Reviews of Modern Physics*, 84(2):621–669, May 2012.

[WSB+04] A Wallraff, D I Schuster, A Blais, L Frunzio, R-S Huang, J Majer, S Kumar, S M Girvin, and R J Schoelkopf. Strong coupling of a single photon to a superconducting qubit using circuit quantum electrodynamics. *Nature*, 431(7005):162–7, September 2004.